Scholar Commons
USF University of South Florida

University of South Florida
Scholar Commons

Graduate Theses and Dissertations | Graduate School

3-10-2016

Production of Biodiesel from Soybean Oil Using Supercritical Methanol

Shriyash Rajendra Deshpande

Follow this and additional works at: http://scholarcommons.usf.edu/etd

 Part of the Oil, Gas, and Energy Commons, and the Statistics and Probability Commons

Scholar Commons Citation
Deshpande, Shriyash Rajendra, "Production of Biodiesel from Soybean Oil Using Supercritical Methanol" (2016). *Graduate Theses and Dissertations.*
http://scholarcommons.usf.edu/etd/6080

This Thesis is brought to you for free and open access by the Graduate School at Scholar Commons. It has been accepted for inclusion in Graduate Theses and Dissertations by an authorized administrator of Scholar Commons. For more information, please contact scholarcommons@usf.edu.

Production of Biodiesel from Soybean Oil Using Supercritical Methanol

by

Shriyash R. Deshpande

A thesis submitted in partial fulfillment
of the requirements for the degree of
Master of Science in Chemical Engineering
Department of Chemical and Biomedical Engineering
College of Engineering
University of South Florida

Co-Major Professor: Aydin K. Sunol, Ph.D.
Co-Major Professor: George P. Philippidis, Ph.D.
John N. Kuhn, Ph.D.

Date of Approval:
March 8, 2016

Keywords: Vegetable Oils, Transesterification, Methyl Esters,
Gas Chromatography, Factorial Design, Supercritical Alcohol

Copyright © 2016, Shriyash R. Deshpande

ACKNOWLEDGMENTS

I would like to thank the faculty members of my committee, Dr. Aydin Sunol, Dr. George Philippidis, and Dr. John Kuhn. The completion of this work would not have been possible without the guidance of Dr. Aydin Sunol whom I thank for his support and motivation throughout the duration of this work. Working with Dr. Sunol has been a great learning experience. I would also like to thank Dr. George Philippidis for his support and his timely advice in moving the project forward on the right path. Dr Philippidis has been an invaluable resource. I would like to extend my acknowledgements to Dr. Laurent Calcul and Andrew Shilling from the Chemodiversity facility (CDDI) for their assistance in sample analysis.

I would like to thank Vignesh Subramanian for assisting me in reviewing the experimental design and its analyses. This work would be incomplete without acknowledging the assistance and support from the other members of the EFES research group. I thank Kyle Cogswell, Aaron Driscoll, Ahmet Manisali and Zachary Cerniga for their assistance throughout the completion of this project.

I would like to thank my parents for giving me an opportunity to pursue my dreams, and supporting me through the ups and downs during the completion of this work. Fruitful research needs patience and dedication. I thank my parents and my brother Yashodhan, for believing in me and for pushing me through the hard times. I owe this accomplishment to your loving support. Last but not the least, I would like to take this opportunity to thank my close friends, Prasad, Abhijeet, Amol, Kaustubh, Bhuvan, Lokesh, Gunjan, Vishal, Vaishnavi, Rishi and Rashmi. Without the strong bonds of our friendship, this work would not have been possible.

TABLE OF CONTENTS

LIST OF TABLES

LIST OF FIGURES

ABSTRACT

The slow yet steady expansion of the global economies, has led to an increased demand for energy and fuel, which would eventually lead to shortage of fossil fuel resources in the near future. Consequently, researchers have been investigating other fuels like biodiesel. Biodiesel refers to the monoalkyl esters which can be derived from a wide range of sources like vegetable oils, animal fats, algae lipids and waste greases. Currently, biodiesel is largely produced by the conventional route, using an acid, a base or an enzyme catalyst. Drawbacks associated with this route result in higher production costs and longer processing times. Conversely, supercritical transesterification presents several advantages over conventional transesterification, such as, faster reaction rates, catalyst free reaction, less product purification steps and higher yields.

This work focused on the supercritical transesterification of cooking oil, soybean in particular. The experimental investigation was conducted using methanol at supercritical conditions. These conditions were milder in terms of pressure than those reported in literature. A batch setup was designed, built and used to carry out the supercritical transesterification reactions. The biodiesel content was analyzed using gas chromatography-mass spectrometry to calculate reaction yields. Methyl ester yield of 90% was achieved within 10 minutes of reaction time using supercritical transesterification. A maximum yield of 97% was achieved with this process in 50 minutes of reaction time. Two key factors, temperature and molar ratio were studied using variance analysis and linear regression and their significance on the biodiesel yield was determined. The kinetic tendency of the reaction was investigated and the values of rate constants, activation energy and the pre-exponential factor were estimated.

CHAPTER 1: INTRODUCTION

The world energy demands are soaring on one hand, while on the other hand the fossil fuel reserves are limited. The markets for petroleum and other liquid fuels have entered a phase of dynamic change, with the supply and demand sides of the chain being unstable. Considering a "high oil price" case, the world crude oil prices will increase in the long run due to the higher demands and lower supplies of crude oil in non-OECD countries. As a result, the weighted average price for U.S. petroleum products is projected to rise by 84% from $3.16/gallon back in 2013 to $5.81/gallon by 2040 [1]. Considering a "low oil price" case, the crude oil prices will go down due to the higher supply from oil producing countries and the lower demand in non-OECD countries. Subsequently, the weighted average price for U.S. petroleum products will drop by 26% from $3.16/gallon in 2013 to $2.32/gallon in 2040. The price for U.S. distillate fuel (diesel) is projected to rise by 23% through 2040, due to the demand in freight requirements and the shift of light-duty vehicles from gasoline to diesel [1]. Figure 1-1 shows the projections of distillate fuel oil prices through 2040 for the "high oil price", "reference", and "low oil price" cases.

With such uncertainty about fuel availability and price in the near future, a dependable liquid fuel is needed that can provide us with energy security, particularly in the transportation sector. Bioenergy can play a major role in replacing fossil fuels and meeting the future demands of the transportation sector. Modern bioenergy resources like biodiesel and ethanol are the prominent biofuels currently in use. Biodiesel seems to be a better option considering the fact that the processing technology for biodiesel is simpler than that of ethanol [2]. The concept itself is

more than a century old, as Dr. Rudolf Diesel, the inventor of the diesel engine had demonstrated the ability of his engine to run on vegetable oil during the Paris Exposition in 1900 [10]. Biodiesel is a derivative synthesized from renewable sources like vegetable oils, animal fats and so on [4].

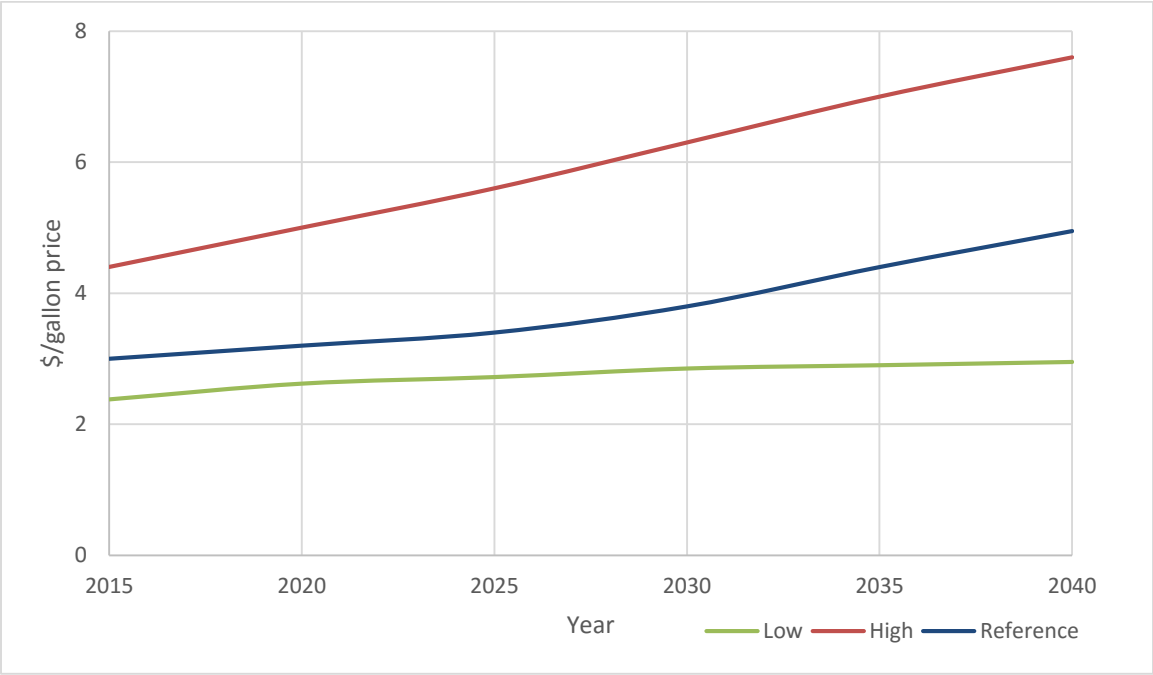

Figure 1-1 Distillate fuel oil price projections in three cases through 2040.(Adapted from [1])

When considering large-scale use of alternative fuels, it is necessary to understand and take into account their production efficiencies. Conventional petroleum based fuels require more energy to produce than what they contain. On the contrary, biodiesel can deliver more energy per unit than the amount of energy required to produce one unit of biodiesel [5]. A life cycle analysis study concluded that biodiesel is capable of delivering 3.2 units of fuel product energy per unit fossil fuel energy spent in its production, as opposed to petroleum diesel, which delivers only 0.83 units of fuel energy per unit of fossil fuel energy consumed [6]. Petroleum diesel and biodiesel production processes are equally efficient in converting raw materials in to usable fuel. But, the fossil fuel energy input is low for biodiesel, since biodiesel can be produced from renewable feedstocks like vegetable oils, algae lipids and animal fats, making biodiesel a truly renewable fuel

[6]. Biodiesel has been gaining popularity over the past few years. The global biodiesel production in 2004 was 2.4 billion liters. This capacity increased to about 26.3 billion liters in 2013 [7]. As seen in figure 1-2, the biodiesel production capacity in the United States has been increasing over the past few years. The U.S. diesel production in 2013 was about 48.2 billion gallons. The U.S. biodiesel production during the same year was about 1.3 billion gallons, which is about 2.6% of the diesel production. Projections to 2040 estimate the U.S. diesel production of about 60.9 billion gallons while that of biodiesel being 2.5 billion gallons. Thus by 2040, biodiesel will represent about 4% of the total diesel fuel produced. One of the most important factors that make biodiesel a primary choice as a biofuel is that biodiesel is compatible with the current diesel engines with little or no modifications [8].

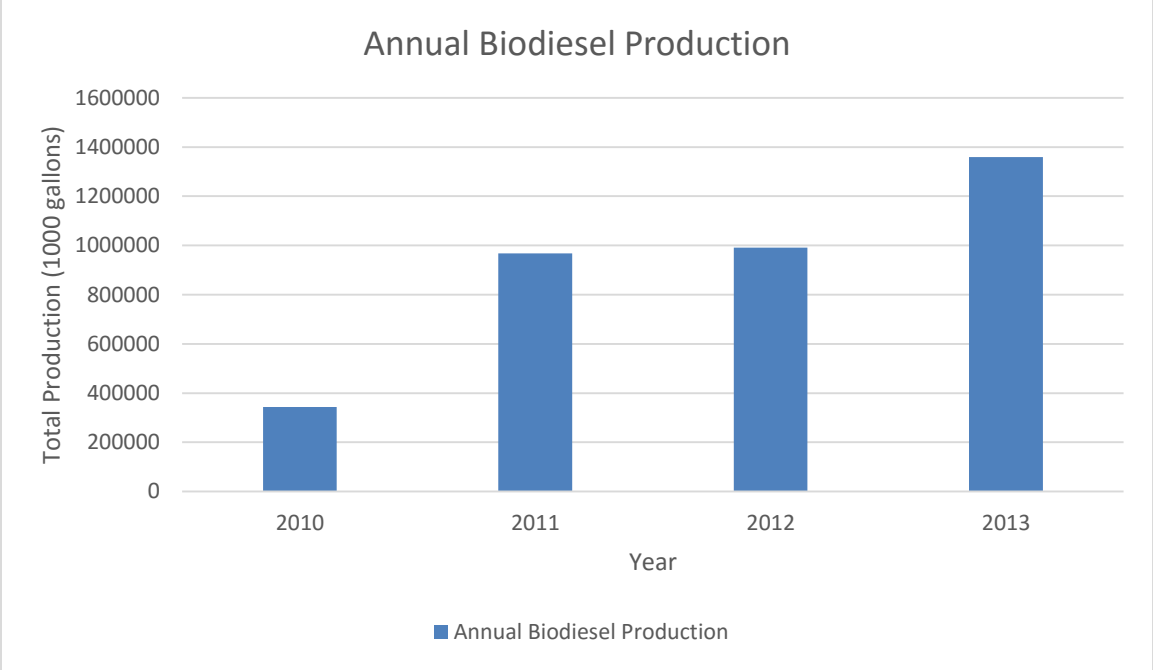

Figure 1-2 Biodiesel production capacities.
(Based on the data from USDA ERS, http://www.ers.usda.gov/data-products/us-bioenergy-statistics.aspx, Table 4)

A number of technologies are available for producing biodiesel from a range of raw materials. The most commonly used approach for commercial biodiesel production is

transesterification [9]. Although, transesterification through the catalyzed route is most commonly used in the industry, this technique does come with a few drawbacks such as, longer processing times, catalyst regeneration and recovery, biodiesel washing, and undesired saponification. Supercritical transesterification on the other hand alleviates the problems faced during catalyzed transesterification, without compromising on the quality of biodiesel.

The main objective of this research was to study the production of biodiesel from cooking oil, in a single catalyst-free step using the supercritical transesterification process. Further, this study also focused on analyzing the biodiesel samples using gas chromatography-mass spectrometry based approach to determine the biodiesel yields. The work in this thesis consisted of the following tasks:

- Designing and building an experimental setup capable of withstanding the supercritical reaction conditions and further fine tuning its performance to conduct a successful experimental study.
- Identifying the key parameters in supercritical transesterification and assessing their effect on biodiesel yield with the least number of experimental runs.
- Developing a GC-MS based analysis method for the determination of methyl ester yields at each of the chosen experimental conditions.
- Analysis of variance and development of a regression model to determine the significant factors affecting the reaction conversion.
- Preliminary estimate of the kinetic tendency of the reaction.

Each of these steps is described in the subsequent chapters, followed by the results and conclusions drawn from the research findings. The next chapter provides in-depth information on the various biodiesel production technologies.

CHAPTER 2: CONVENTIONAL BIODIESEL PRODUCTION TECHNOLOGIES

Vegetable oils are the most widely used raw materials for biodiesel production. The fact that vegetable oils are renewable and have an energetic content close to diesel fuels make them an attractive raw material for biodiesel [10]. Vegetable oils can be directly used with diesel engines, but certain drawbacks make them unsuitable for use over a prolonged period. Techniques like pyrolysis (or thermal cracking), microemulsions and transesterification can be used to convert vegetable oils to biodiesel. The following sections give in-depth information on each of these methods, and their merits and challenges.

2.1 Direct Use of Vegetable Oils

Vegetable oil was proposed to be used as an alternative to petroleum in the 1980's [11]. Vegetable oils have a high heat content (about 88% of D2 fuel), they are biodegradable, have low aromatic content and are readily available. But on the downside, they have high viscosities, lower volatilities and the unsaturated hydrocarbon chains are reactive. Although, vegetable oil can be directly used in compression engines for a short term, its long term use poses many problems. The major problem arises from the high viscosity of vegetable oil [3]. In long term engine tests, injector coking, higher carbon deposits, sticking of piston rings, thickening and gelling of engine lubrication oil and other issues have been reported [3,12].

2.2 Pyrolysis

Pyrolysis or thermal cracking involves the breaking of long chains of carbon-, hydrogen- and oxygen- containing compounds (mainly biomass) into smaller molecules at high temperature and in the absence of oxygen. A wide range of raw materials, like vegetable oils, animal fats, and

natural fatty acids can be pyrolyzed. The organic components in these materials start decomposing at around 350 °C – 550 °C in the absence of oxygen, and continue decomposing as the temperature rises up to 700 °C – 800 °C [13]. Pyrolysis studies were reported in literature as early as 1947. Tung oil calcium soaps were subjected to thermal cracking to yield crude oil. The crude was further refined to produce diesel fuel, gasoline and kerosene [14].

Based on the operating conditions, pyrolysis can be classified as conventional (slow) pyrolysis, fast pyrolysis and flash pyrolysis. Conventional pyrolysis is carried out at 276 °C – 676 °C. The process is characterized by long gas residence times (7-8 minutes) and low heat transfer rates, which affects the quality of the fuel produced. Fast pyrolysis is characterized by high heat transfer, high heating rates, and short residence times. The reaction occurs within the temperature range of 576 °C – 976 °C [13]. In case of flash pyrolysis, the reactants undergo rapid devolatilization at temperatures to the order of 776 °C – 1026 °C. Flash pyrolysis is characterized by very short gas residence times (less than 1 second) and high heating rate of particles [15]. Even though the process is fast, it has some technological shortcomings like poor thermal stability, presence of solids in the oils, corrosive nature of oil, dissolved char in oil and the production of pyrolytic water as a by-product [16]. Since pyrolysis undergoes various reaction pathways and a variety of reaction products can be obtained from pyrolysis, pyrolytic chemistry is rather difficult to characterize [4].

2.3 Microemulsions

A microemulsion can be defined as a clear and thermodynamically stable dispersion of two immiscible liquids, which contains a certain amount of surfactant or a surfactant and a co-surfactant [17]. Microemulsion droplets are small with diameters within the range of 100 to 1000 °A. Vegetable oils with an ester or a dispersant, or a vegetable oil, alcohol and a surfactant could

form a microemulsion. Although the presence of alcohol in the microemulsion improves latent heat of vaporization and cools the combustion chamber, reducing the nozzle coking effect, microemulsions have lower volumetric heating values as compared to diesel [18].

Ziejewski et al., prepared a microemulsion with 53.3% of alkali refined and winterized sunflower oil, 13.3% of 190-proof ethanol and 33.4% of 1-butanol. In their engine tests they found that the fuel mass ratio increased due to higher density and viscosity of the microemulsion. Since the heating value of the microemulsion was 19% lower than that of diesel, a lower energy input and consequently a lower power output was observed. One of the major problems reported was the difficulty in starting the engine even at room temperature [19]. Although microemulsions show a considerable promise as low viscosity fuel blends with vegetable oils, their cetane numbers are lower and they have low heating values as compared to D2 grade diesel fuel [20].

2.4 Transesterification

Transesterification is a reaction where one ester is transformed into another ester by the interchange of the alkoxy moiety [21]. The process is also known as alcoholysis, since the alcohol from the ester is replaced by another alcohol. The process is similar to that of hydrolysis, except the fact that an alcohol is used instead of water [22]. Figure 2-1 represents the general mechanism of transesterification.

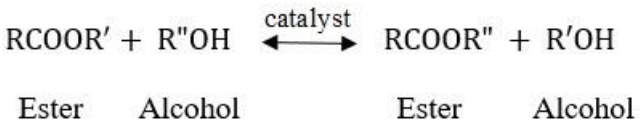

Figure 2-1 General transesterification mechanism.

When triglycerides are subjected to transesterification, the reaction yields fatty acid esters (of the respective alcohol reacted) along with glycerol as the by product. The reaction proceeds in three steps, with diglycerides and monoglycerides forming in subsequent steps and finally the

esters along with glycerol in the last step [23]. The mechanism of transesterification is discussed in detail in chapter 3. More than often the transesterification reaction is catalyzed by bases [24], acids [25] or enzymes [26].

2.4.1 Base-Catalyzed Transesterification

The most commonly used commercial process for biodiesel production is base-catalyzed transesterification. This is due to the fact that base-catalyzed transesterification reactions proceed at considerable faster rates as compared to acid-catalyzed transesterification reactions. Also, base catalysts are far less corrosive to the equipment than acid catalysts [27]. Although base catalysts like sodium hydroxide (NaOH) and potassium hydroxide (KOH) are widely available and inexpensive, their ability to catalyze transesterification is limited when the oil has a high free fatty acid (FFA) content [28]. FFA's are made up of a long carbon chain disconnected from the glycerol backbone. The alkali catalyst can react with the FFA to form soap [29]. This side reaction is undesirable since soap formation hinders the production of fuel grade biodiesel, resulting in high product separation costs. Although homogenous base catalysts are able to catalyze the transesterification reaction at low reaction temperature and atmospheric pressure, are widely available and inexpensive, and produce high yields, their use is limited to the oils where the FFA content is no more than 0.5% by weight [30] and acid value less than 1 mg KOH/g [31].

Solid base catalysts, also known as heterogeneous base catalysts like basic zeolites, alkaline earth metal oxides and hydrotalcites have been developed and used for biodiesel production in the past. Alkaline earth metal oxides like calcium oxide have recently attracted much attention since it possesses high basicity, dissolves very slowly in alcohol and can be synthesized from relatively inexpensive sources like limestone and calcium hydroxide [32]. Although these catalysts separate easily from the liquid reaction products since they are in solid form, an extra

purification step may be needed in certain cases. Some researchers have found that these catalysts can dissolve to some extent in the reaction products and may form other compounds, for example, calcium oxide can react with glycerol to form calcium diglyceroxide, which is soluble in biodiesel [33]. Further, catalysts like calcium oxide are rapidly hydrated in air. The catalyst may undergo poisoning due to the chemisorption of water and carbon dioxide on the active surface sites, affecting the performance of the catalyst. Magnesium oxide (MgO) is among the other options for heterogeneous base catalysts. It can be synthesized by direct heating of magnesium carbonate or magnesium hydroxide and can catalyze the transesterification reaction, but only at higher reaction temperatures (above 180 °C) [34]. At lower reaction temperatures and pressures, the catalyst loses its activity [32]. Strontium oxide is another metal oxide that is highly active. Although it is soluble in the reaction medium, research suggests that using just 3% catalyst by weight, the reaction can produce 90% yields of methyl esters in 30 minutes at 65 °C, even with the specific surface area of the catalyst being as small as 1.05 m^2/g [35].

2.4.2 Acid-Catalyzed Transesterification

Liquid base-catalyzed transesterification has certain limitations with respect to the presence of free fatty acids (FFA's), soap formation and catalyst separation. To overcome these limitations, liquid acid catalysts have been proposed for the transesterification reaction. Sulfuric acid (H_2SO_4) and hydrochloric acid (HCl) are the most commonly used homogeneous acid catalysts [32]. It has been reported that acid catalysts can be used where the free fatty acid content of the raw material is higher. In other words, unlike alkali catalysts, acid catalysts do not get affected by the presence of free fatty acids [27]. On the downside, acid-catalyzed transesterification reactions have slower reaction rates with relatively lower conversion ratios,

need a catalyst separation step, and have environmental as well as corrosion related problems [29,30].

Due to these limitations, researchers focused on exploring solid or heterogeneous acid catalysts for transesterification. Solid acid catalysts are unaffected by the presence of free fatty acids (FFA's), can catalyze esterification and transesterification reactions simultaneously [36], are easy to separate from the reaction products, regenerate and recycle, and reduce the problems associated with corrosion even in the presence of acid species. A solid acid catalyst having an interconnected porous structure with a high concentration of acid sites and a hydrophobic surface is ideal for transesterification. The pore system minimizes the diffusion problems for molecules with larger chain structures and the high concentration of acid sites helps the reaction to proceed at faster rates [28].

Catalysts like zirconium oxide (ZrO_2), titanium oxide (TiO_2), tin oxide (SnO_2), zeolites and ion exchange resins have been shown to be effective for transesterification. Moreover, modifying the metal oxide surface acidity has shown to improve the transesterification yields [29]. For example, sulfated zirconia (SO_4^{2-}/ZnO_2) was found to produce methyl ester yields as high as 90.3% and 86.3% in the transesterification of palm kernel oil and crude coconut oil respectively, as compared to 64.5% and 49.3% when unsulfated ZnO_2 was used [37]. But catalysts like SO_4^{2-}/ZnO_2 are prone to deactivation due to sulfate leaching. This will effectively cause transesterification by the homogeneous route and will interfere with the measurements of heterogeneous catalytic activity. Catalysts like TiO_2 have been evaluated for transesterification. Although SO_4^{2-}/ TiO_2 was found to achieve a yield of 90%, the reaction is slow and requires high temperatures as compared to base catalyzed transesterification [29].

2.4.3 Enzyme-Catalyzed Transesterification

Enzymes can be used to catalyze the transesterification reaction. Both intracellular and extracellular lipases can be used for enzymatic production of biodiesel. In both cases the enzyme is immobilized to be reused. Also, immobilizing the enzyme eliminates the issues with catalyst separation from final products [38]. Extracellular lipases like *Mucor miehei* and *Candida antarctica* (Novozym 435) have been used for transesterification of sunflower oil with primary alcohols like methanol and ethanol [39]. The ester yields were found to be around 70% with methanol and 72% with absolute ethanol.

This process operates at a much lower temperature (50 °C) as compared to other processes. On the downside, the commercial application of enzyme catalyzed transesterification is limited due to the fact that the costs of these catalysts per kg ester produced are high compared to those of alkali catalysts. Slow reaction times and low yields also limit enzymatic transesterification [40]. Enzyme catalyzed transesterification remains an active area of research wherein researchers are focusing on improving the yields and minimizing the reaction times. From the studies so far, vast data have been collected and the efforts to optimize the process continue. Along with optimization, focusing on other aspects like efficient recovery and utilization of glycerol byproduct can make the process economically feasible and environmentally friendly [40].

CHAPTER 3: BIODIESEL PRODUCTION USING SUPERCRITICAL FLUID TECHNOLOGY

3.1 Supercritical Fluids

Supercritical fluids date back to the discovery of the critical point by Baron Cagniard de la Tour in 1822. In his experiments, he found that the gas-liquid phase boundary disappeared when materials were heated above a certain temperature [41]. A supercritical fluid can be defined as any substance whose temperature and pressure are higher than their critical values and which has a density close to or higher than its critical density [42]. This temperature and pressure are referred to as the critical temperature (T_c) and the critical pressure (P_c) respectively, which are the coordinates of the critical point on the phase diagram. Figure 3-1 shows the phase diagram for a pure substance.

As the temperature and pressure increases, the fluid reaches the critical state, and beyond the critical point the distinction between liquid and gas phases disappears. This is the supercritical fluid region. It is in this region that the fluid exhibits both gas-like and liquid-like properties and exists as a non-condensable dense fluid whose density ranges from 20 to 50% of that in the liquid state and its viscosity is close to that in its gaseous state [43]. The properties of these fluids are tunable and can be adjusted to be liquid-like or gas-like, by changing the pressure or temperature, without crossing the phase boundary [44]. Table 3-1 shows a comparison between typical values of physical properties of gases, liquids and supercritical fluids.

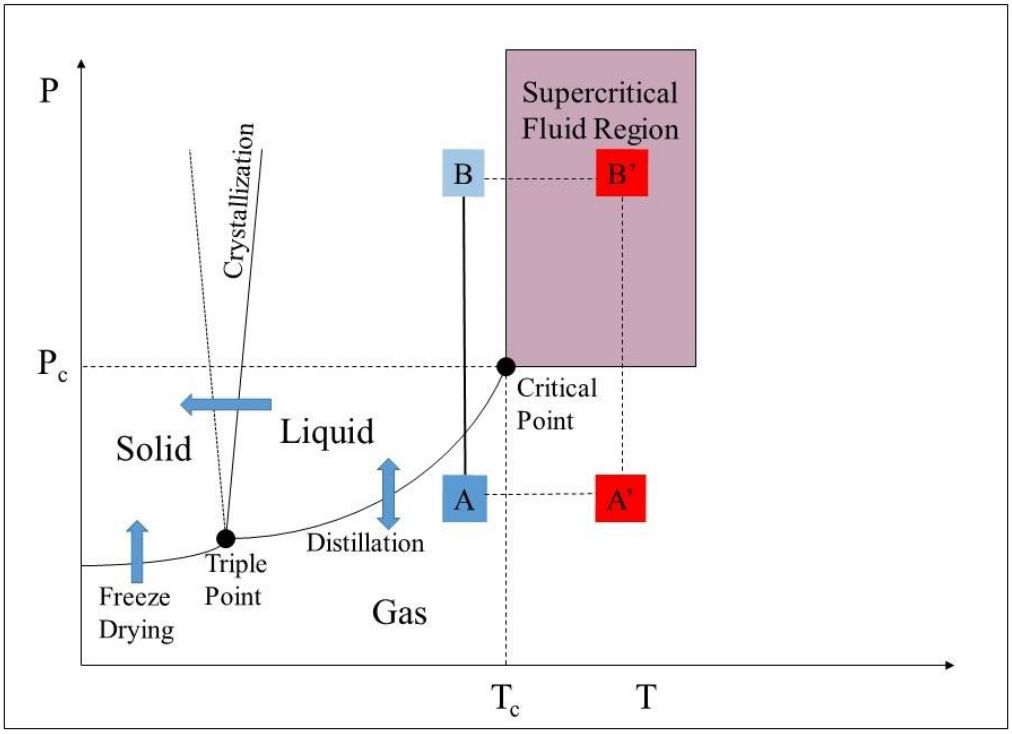

Figure 3-1 Schematic phase diagram for pure fluid in supercritical state. (Adapted from [83])

Table 3-1 Comparison of typical values of transport properties of gases, supercritical fluids and liquids (Adapted from [84])

State	Defining Condition	Property		
		Density (kg/m^3)	Diffusivity (m^2/s)	Viscosity ($kg/m{\cdot}s$)
Gas	1 atm, 25 °C	0.6 - 2	$1 - 4\times10^{-5}$	$1 - 3\times10^{-5}$
Liquid	1 atm, 25 °C	500 - 1600	$0.2 - 2\times10^{-9}$	$0.2 - 3\times10^{-3}$
SC Fluid	T_c, P_c	200 - 500	$0.5 - 4\times10^{-7}$	$1 - 3\times10^{-5}$
SC Fluid	T_c, $4P_c$	400 - 900	$0.1 - 1\times10^{-7}$	$3 - 9\times10^{-5}$

Although the supercritical region is shown to have marked boundaries in the figure, in practice this is not entirely true. The areas to the left of the supercritical region as well as below the supercritical region are equally important in supercritical processes. It can be observed that there are no phase boundaries in these areas. The conditions here correspond to pressures and temperatures lower than their critical counterparts, but are equally important. The fluids in these

regions are referred to as near-critical fluids or subcritical fluids [45]. As seen in the figure, the isotherm below the critical region (isotherm AB) involves phase transition, while the isotherm above the critical region (isotherm A'B') is a single phase with no phase transitions [83].

Supercritical fluids have promising applications in many fields including but not limited to chemical processing, extraction, chemical reactions, waste treatment, recycling, pollution prevention, and others. The book, "Supercritical Fluids – Molecular interactions, physical properties and new applications" illustrates some of the most important and useful applications of supercritical fluids and the technology itself, focusing on the key areas of extraction and separation, material processing, and reactions [46].

3.2 Supercritical Transesterification

Before supercritical transesterification came into picture, researchers investigated the transesterification of soybean oil in the absence of a catalyst, under subcritical conditions. They reacted methanol with soybean oil at 220-235 °C, 55-62 bar and 6:1-27:1 mol/mol ratio [47]. They were able to achieve methyl ester yields of about 85 weight percent after 10 hours of reaction time at 235 °C. Thus, it was concluded that transesterification was possible even without using catalysts, with the downside being slow reaction rates. Although, triglyceride and diglyceride conversion rates were high, monoglyceride to glycerol conversion rates were found to be very slow [47]. Then in 2001, Saka and Kusdiana pioneered the technique of producing biodiesel using supercritical transesterification. They reacted rapeseed oil with methanol under supercritical conditions (350 °C and 45-65 MPa) to produce methyl esters. The reaction was completed within 6 minutes with about 95% conversion to methyl esters [48].

The reaction mechanism of supercritical transesterification is predicted to be similar to that of acid-catalyzed transesterification. In case of methanol (or any other alcohol at supercritical

conditions), the hydrogen bond is weakened at higher temperatures. However, while acid-catalyzed transesterification is a much slower process even in comparison with base-catalyzed transesterification, the supercritical transesterification process on the other hand is much faster in terms of complete conversion of the triglycerides to esters [43]. This can be attributed to the fact that the hydrogen bonding between OH oxygen and OH hydrogen, which forms methanol clusters, decreases with increasing temperature, thereby decreasing the polarity of methanol in the supercritical state. Thus non-polar triglycerides can get solvated in supercritical methanol, forming a single phase of oil and methanol. This phenomenon results in accelerated kinetics under supercritical conditions [49]. Table 3-2 shows the typical reaction conditions for the catalyzed processes in comparison with the supercritical methanol process.

Table 3-2 Comparison of transesterification processes

Process	Temperature (° C)	Pressure (psi)	Reaction Time	Molar Ratio (MeOH:Oil)
Base Catalyzed	60 – 90	Atmospheric	0.5 – 2 hours	6:1 to 18:1
Acid Catalyzed	65 – 200	Atmospheric	4 – 70 hours	6:1 to 30:1
Enzyme Catalyzed	35 – 40	Atmospheric	7 – 72 hours	3:1 to 4:1
Supercritical	300 – 340	Above 1200	5 – 10 minutes	42:1

Note: The table represents conditions for biodiesel yields of 90% and above

The reaction mechanism has been studied by many researchers. For alcohol to oil molar ratios below 24:1, it is assumed that the supercritical transesterification reaction proceeds in three irreversible steps. The kinetic model is based on the concentrations of both the triglyceride and the alcohol [47,50]. In the first step, since the reaction conditions are supercritical, the hydrogen bond energy is lowered, allowing the alcohol molecule to be a free monomer. The alcohol molecule attacks the carbonyl carbon of the triglyceride molecule. In the case of methanol, it leads to the formation of a diglyceride along with a molecule of fatty acid methyl ester. A similar mechanism is applicable to the second step, where the diglyceride reacts with a methanol molecule to form a

monoglyceride and a second molecule of fatty acid methyl ester. In the final step, the monoglyceride reacts with methanol to produce glycerol and a third molecule of fatty acid methyl ester [43]. Figure 3-2 represents the three-step mechanism. Although the overall reaction is predicted to be reversible, for higher molar ratios the reversible reaction can be ignored and the methanol concentration can be considered to remain constant [51]. The reaction is assumed to follow first order rate-law as a function of triglyceride concentration, so the reaction mechanism is condensed into a single step, ignoring the concentrations of the intermediates [49, 51].

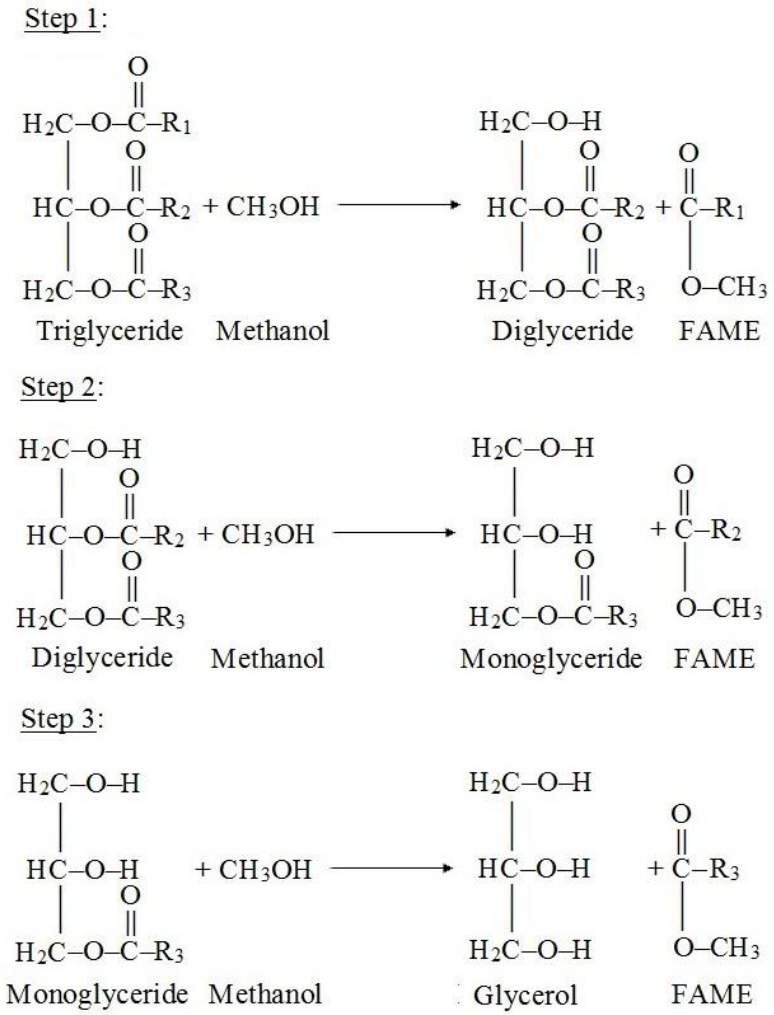

Figure 3-2 Three step transesterification mechanism

3.3 Advantages and Disadvantages of Supercritical Transesterification

In the case of conventional catalyst-based transesterification, product separation and catalyst recovery are the most energy intensive stages, and consequently economically unfavorable [52]. Since supercritical transesterification does not rely on catalysts, it completely eliminates the problems faced during catalyzed transesterification, thereby reducing the cost of separation and purification of final products [53]. The supercritical transesterification reaction is completed within minutes as compared to the base-, acid-, or enzyme-catalyzed processes that take hours [48,54]. When considering biodiesel production methods, it is essential to take into account the flexibility of the feedstock that can be processed using those methods. As compared to the conventional base-catalyzed process, the supercritical process is more tolerant to the presence of water and free fatty acids [36]. In fact, it was found that the presence of water positively affected the formation of methyl esters by supercritical transesterification [55]. Thus supercritical transesterification can also be used with low grade or moisture containing feedstocks [56]. Thus the steps for feedstock pretreatment like moisture and free fatty acid removal as well as post production treatments like washing, drying and catalyst removal are not needed. This results in supercritical transesterification having much higher production efficiency than the conventional catalytic processes [43].

On the downside, supercritical transesterification does require higher temperatures, higher pressures and higher molar ratios, resulting in higher capital and operating costs [57]. Due to the higher molar ratios, the preheating and recycling steps become energy intensive. The presence of higher amount of alcohol in the products slows down the biodiesel-glycerol phase separation [43]. In a techno-economic study by Marchetti and Errazu, simulation models were employed to analyze the productivity, raw material requirements, environmental impacts and economic advantages of different processes for biodiesel production. They concluded that although supercritical

transesterification technology has the most technical advantages, it also has the highest capital investment compared to the other available technologies, as well as the highest cost per kilo of biodiesel produced [58]. However, taking advantage of heat integration opportunities it is possible to reduce the energy demands for this process and improve its economic feasibility [43].

CHAPTER 4: FEEDSTOCKS FOR BIODIESEL PRODUCTION

The cost of biodiesel is largely dependent on the cost of feedstock. The cost of feedstock accounts for about 88% of the total production costs [59]. The dependence of production costs on the costs of feedstock was analyzed by Haas et al., who indicated the existence of a direct linear relationship between the two, such that a US$ 0.075/gal change in product cost was caused by a US$ 0.01/lb change in the feedstock cost. This makes the choice of feedstock critically important. Furthermore, it signifies the need to develop technologies such as supercritical transesterification, which can handle lower quality inexpensive feedstock without affecting the quality of biodiesel produced.

Biodiesel feedstocks can be classified as first generation, second generation and third generation feedstocks. Feedstocks of edible oils like rapeseed, soybean, palm and sunflower fall under the first generation feedstock category, primarily because these were the first oil crops to be used as feedstock for biodiesel synthesis [60]. Alternative non-edible sources like oil crops of jatropha, tobacco seed, jojoba oil, salmon oil, mahua, and seamango are categorized as the second generation feedstocks [60]. This category also includes used cooking oils, restaurant greases, and animal fats [61]. The second generation feedstock reduce the dependence of biodiesel production on the edible oils. The third generation biodiesel feedstock are lipids derived from microalgae [60]. Since microalgae have sustainability advantages over the first and second generation feedstocks, interest in using microalgae for biodiesel production has been growing over the years. This section will stress upon the currently available feedstocks in the market.

4.1 Vegetable Oils

The original diesel engine was designed to run on vegetable oil. Eventually, vegetable oils were used to synthesize biodiesel via transesterification [54]. Vegetable oils are composed of about 98% triglycerides and the rest being mono- and diglycerides [62]. The triglyceride molecule is the major component of vegetable oils, consisting of three esters of the fatty acid chain attached to a backbone of glycerol [63]. Depending on the region of production and the climate in that area, the type of vegetable oil used may vary. Soybean oil is prevalent in the United States, rapeseed oil in Canada and the European nations, and palm oil in Malaysia, Indonesia and Latin America [63].

Although vegetable oils are abundantly available, they represent a major food staple and their use for biodiesel production competes with their primary use as food sources, giving rise to "food vs fuel" concerns. A solution to this problem is to utilize the used cooking oils and other non-edible oils as raw material sources. Large amounts of used cooking oils are available around the world. According to the projections of the Energy Information Administration, about 100 million gallons of waste cooking oil is produced in the United States every day [64]. Theoretically, this amount can produce about 99.5 million gallons of biodiesel per day, which translates to 36.3 billion gallons of biodiesel produced annually. If the potential of available used cooking oil is fully utilized, the biodiesel obtained can replace more than 50% of the diesel fuel in comparison with the projections of 2040 (60.9 billion gallons). Thus, there is a huge potential in utilizing the used cooking oils for producing biodiesel. Further, the disposal and management of used oils is a challenge in itself due to the possibility of contamination of water and land resources. Using these oils for biodiesel production would provide a solution to their disposal as well as to the food versus fuel debate. The large-scale availability of restaurant oil waste can reduce the overall production costs and significantly enhance the economic viability of biodiesel [61,64].

One critical consideration while selecting used or waste cooking oils as biodiesel feedstock is the change in oil properties due to cooking, which may affect the quality of the final product. During the frying process, the oil undergoes thermolytic, oxidative and hydrolytic reactions. Many undesirable volatile compounds are formed due to the combined effect of these reactions. These compounds could affect the properties of biodiesel or could affect the transesterification reaction itself. Repetitive heating cycles during frying increase the polar content of oil, negatively affecting the biodiesel quality. [36,65,66]. Hence, it is essential to know the amount and the type of these undesirable compounds. Usually, high-performance size exclusion chromatography is used to examine such oil fractions. Some pretreatment is needed to remove these compounds from the oil. Thus, an additional cost with waste cooking oil is the pretreatment step. With that being said, waste cooking oil is still an economical source for biodiesel production [36].

4.2 Animal Fats

The greases primarily collected from animal meat-processing facilities refer to animal fats [61]. Wastes generated by the meat processing industries are inexpensive, as a result of which the interest in producing biodiesel from fats of animal origin like beef tallow and pork lard has increased [67]. Animal fats have similar chemical structures to vegetable oils, but the fatty acids are distributed in a different way. They are a promising source of feedstock for biodiesel production, but have not been as extensively studied as vegetable oils [68]. Although animal fats like pork lard, beef tallow and chicken fat can be used as raw materials to produce biodiesel by conventional transesterification methods, their yields are limited due the significant presence of FFA's in animal fats. [28]. Higher FFA content leads to soap formation in the presence of base catalysts, making product separation costly and reducing the overall efficiency of the process [69].

Supercritical transesterification has shown to address these issues. Past research indicates that supercritical methanolysis of chicken fat at 350 °C was able to produce FAME yields up to

80%. Although, these yields are valid for shorter residence times and molar ratios up to 9:1, they are still significant, given the fact that chicken fat had a much higher free fatty acid content as compared to soybean oil. It was observed that, under longer residence times and higher molar ratios, the fatty acid methyl esters were subject to thermal decomposition. This was evident from the brownish color of the sample and the decrease in the FAME yields for reactions longer than 7 minutes [69]. Biodiesel synthesized from animal fats has its own advantages and disadvantages. Although it has a high cetane number, it is more vulnerable to oxidation since animal fats lack the presence of natural antioxidants [70]. Biodiesel obtained from fats like tallow have a lower flash point and lower heating values. Furthermore, it also has a lower pour point which makes its use in cold weather conditions difficult [71].

4.3 Microalgae

Microalgae consist of both groups of photosynthetic microorganisms; those that have cell walls, nucleus, chloroplasts and mitochondria (eukaryotic) and those that do not (prokaryotic). They grow rapidly, can sustain harsh conditions and are rich in lipids [72]. Depending on the strain of the microalgae, the lipid content can be as high as 80% of the total dry weight. A significant portion of these lipids can be extracted using various extraction techniques. Up to 80% of this lipid mass consists of triacylglycerols (TAGs) [73]. These TAGs can be converted to biodiesel via the transesterification process. Microalgae can be cultivated in brackish or salt water as opposed to potable water and on non-arable land. Moreover, microalgae have high growth rates and productivity as well as high photosynthetic efficiency to produce biomass. Thus, they represent a promising feedstock source for producing biodiesel [60].

Microalgae require a series of pretreatment and processing steps before the lipids in them can be converted to biodiesel. Figure 4-1 shows the microalgae pretreatment flowchart. The process starts with the cultivation of microalgae in open ponds or closed bioreactors, followed by

harvesting and dewatering of the algae [74]. Various separation methods like centrifugation, flocculation, filtration [75], gravity sedimentation, floatation and electrophoresis [76] are used to reduce the water content of the algae, there by concentrating them.

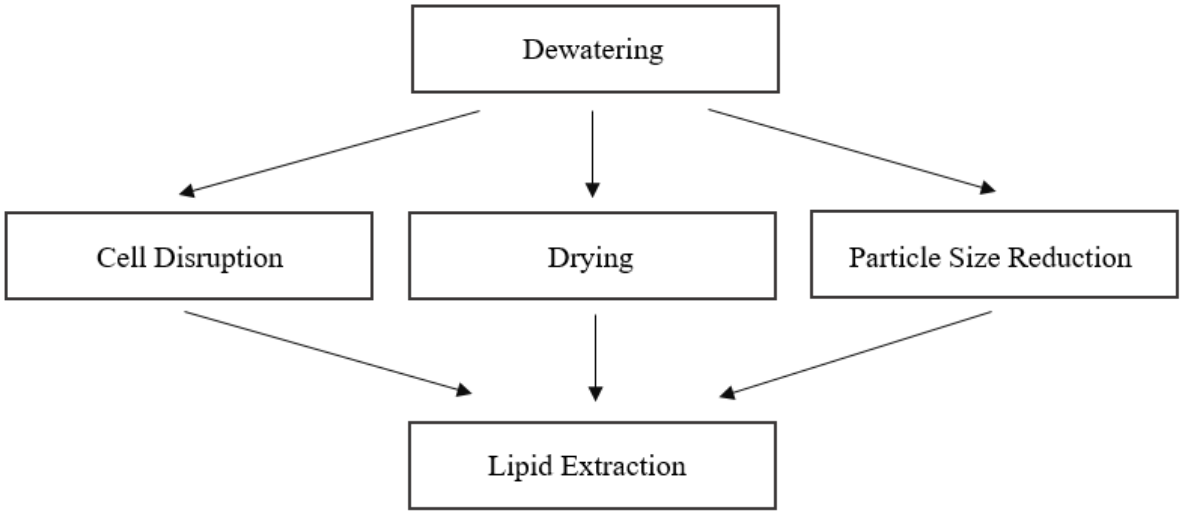

Figure 4-1 Microalgae pretreatment flowchart. (Adapted from [75])

About 60% of the total energy spent in algal biodiesel production is consumed by the dewatering stage itself [77]. After dewatering, the algae need to undergo a pretreatment step which improves the efficiency of lipid extraction. This step primarily involves cell disruption by various techniques to release the intracellular lipids in to the surrounding media [75]. The lipids can be then extracted by either using organic solvents or supercritical fluids and subsequently converted to biodiesel by transesterification.

The environmental impact and the energy burden of microalgal biodiesel production can be understood with the help of the energy efficiency and the fossil energy consumption. The table below compares the energy efficiency and fossil energy consumption for petro-diesel, biodiesel produced from second generation feedstocks, and biodiesel produced from microalgae, where, the

energy efficiency is defined as the ratio of biodiesel fuel energy (calorific value) to the total energy (biomass calorific value and fossil consumption) consumed for production, and the fossil energy consumption is defined as the ratio of the energy derived from the final fuel product to the fossil energy consumed for production [77].

Table 4-1 Comparison of energy efficiency and fossil energy consumption between feedstocks (Adapted from [77])

Feedstock Type	Microalgal oil	Jatropha oil	Used oil	Petrodiesel
Energy efficiency (%)	39.14	35	55	79
Fossil energy consumption (MJ fossil energy/MJ final energy)	0.74	0.58	0.43	1.26

As seen in table 4-1, although the fossil energy consumption of microalgal biodiesel is much lower than that of diesel, it is higher when compared to those of the second generation feedstocks like jatropha oil and used oil. Moreover, microalgal biodiesel has lower energy efficiency as compared to biodiesel derived from used oil. This can be attributed to the multi-step production process and energy intensive preprocessing steps [77]. Moreover, the oil content in the microalgae and the productivity of the strain directly affects biodiesel production and the associated costs. Hence it is important to take these factors into consideration [72].

Thus, even though microalgae represent a potentially sustainable source of feedstock for biodiesel production, the energy demands associated with microalgal biodiesel production are extensive and limit the technology from being scaled up, at least in its current from [78]. The energy and environmental assessments show that the microalgal biodiesel suffers from serious bottlenecks at its current level of maturity. That being said, the future efforts towards microalgal biodiesel production should focus on selection of strains with high lipid content and those that have high rates of productivity and on developing energy efficient dewatering and extraction processes [77, 78].

CHAPTER 5: EXPERIMENTAL WORK

This study used a pilot scale batch reactor setup. Pilot scale experiments allow for a stable experimental environment, which can be tuned, improved and studied. Further, pilot scale experimental setups are larger in capacity as compared to laboratory scale experimental setups. Using such a setup allows us to determine the scalability of the process. The main focus of this work was to produce biodiesel using supercritical transesterification and to study the effects of different reaction parameters on the biodiesel yields. Construction of a reaction setup that could withstand the harsh reaction conditions was a key element. This section describes the overall reaction setup, the equipment and materials used, the experimental procedure and the analysis procedure.

5.1 Experimental Setup and Equipment

The main reaction vessel (autoclave) was obtained from Autoclave Engineers, with SS-316 construction, rated for 9100 psi at 720 F. A magnetic drive stirrer with variable speed control was mounted on the autoclave to keep the contents of the reaction vessel well mixed. The autoclave was fitted with a safety head assembly (rupture disc) capable of venting the reaction contents in case of pressure buildup in excess of 5000 psi. The autoclave was heated using a jacketed heater controlled by the Autoclave Sentinel series temperature controller. The heating jacket covered only the lower 2/3rd of the autoclave. Hence, to keep the conditions isothermal, the upper 1/3rd including the head of the autoclave was wrapped with heating tape obtained from Omega Engineers. The heating tape was rated up to 400 °C and the temperature on the tape was controlled by the Omega

Platinum series temperature controller via a solid state relay (also from Omega Engineers). A dip tube, along with an isolation and cool-down chamber, was installed on the autoclave to draw out the sample. Figures 5-1 and 5-2 show the autoclave assembly, the heating tape assembly, the Magnedrive assembly and the sampling chamber. A spray nozzle was used to disperse the oil flow in the autoclave, to allow for better mixing and higher surface area for the reaction to occur. The nozzle is shown in figure 5-3.

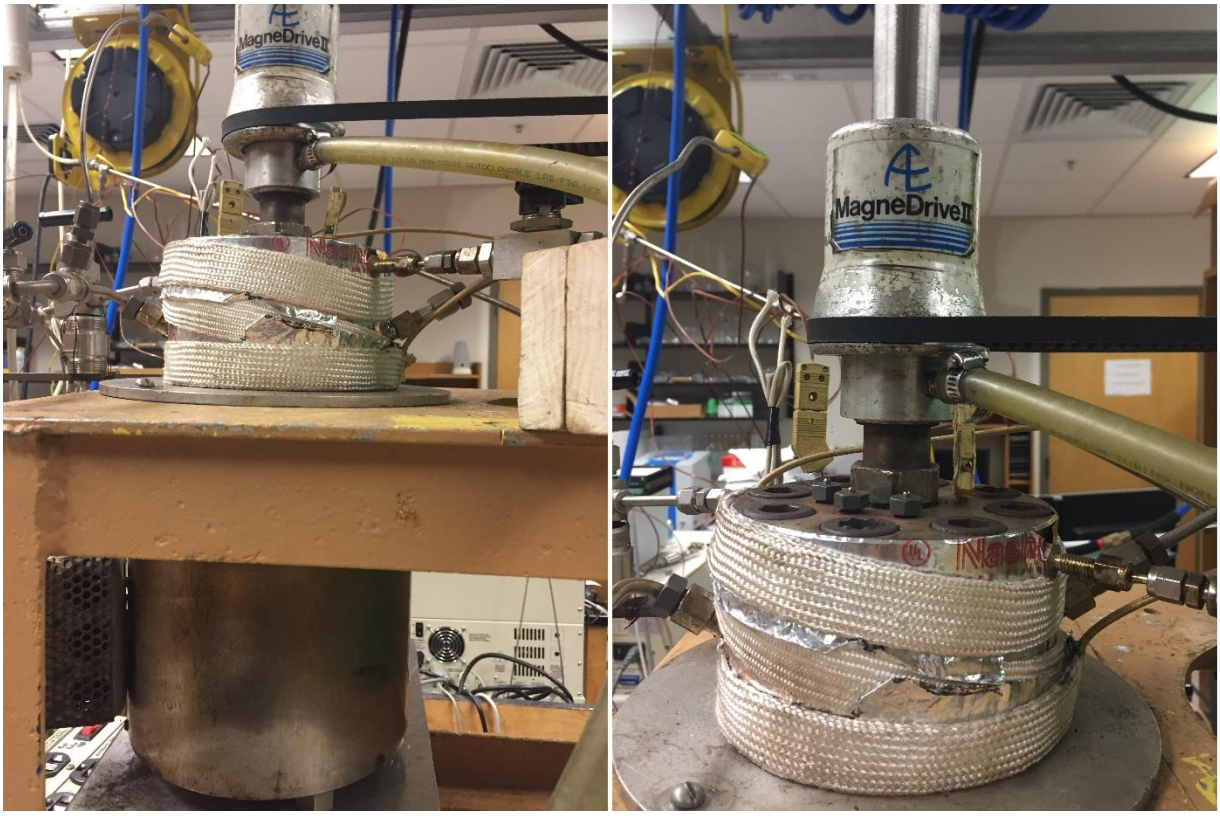

Figure 5-1 Autoclave, heating tape and Magnedrive assembly.

Two separate syringe pumps, from Teledyne ISCO were used for pumping the oil and methanol into the reactor. The pumps are capable of producing pressure up to 5000 psi, while operating under constant flow or constant pressure modes. A fluidized sand bath (from Techne-VWR International) with four 1-kW heaters was used to preheat the oil before exposing it to supercritical methanol in the autoclave. The sand bath was provided with a 4-psi regulated air

supply, which kept the sand fluidized and isothermally heated. The sand bath was mounted on a hydraulic floor jack which allowed to raise and lower the sand bath when needed. Helical coiled ¼ inch Swagelok stainless steel tubing was used for the preheating section. The coil was fixed in position such that the sand bath could be raised on the hydraulic jack to allow the coil to be dipped entirely in the hot fluidized sand.

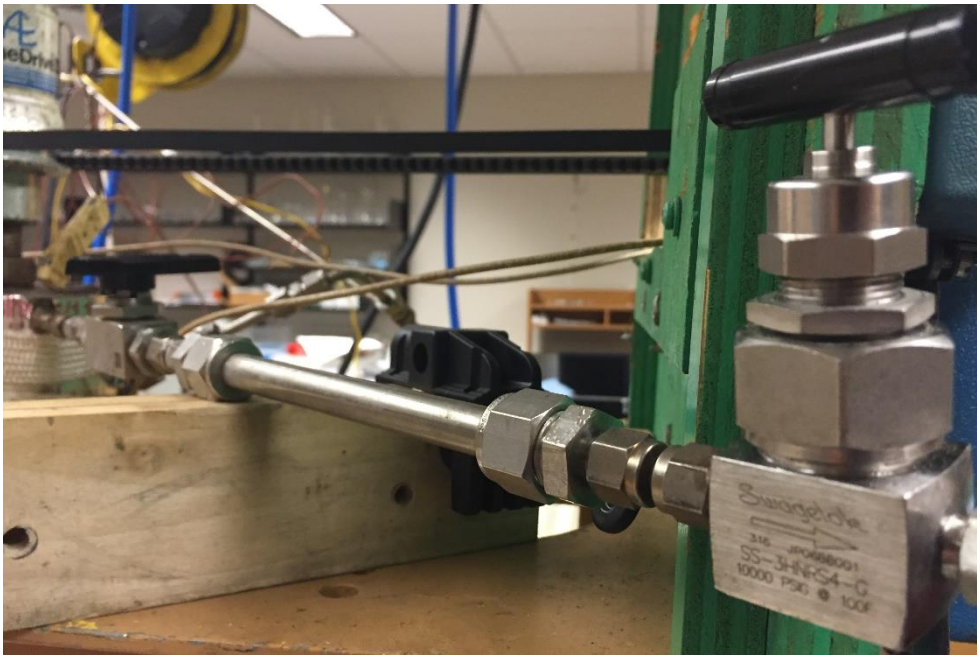

Figure 5-2 Sampling chamber.

To prevent heat loss during the oil flow from the preheating section to the autoclave, another heating tape regulated by a variable transformer was used. The pressure and temperatures on the autoclave were monitored with a Matheson pressure gauge and Omega K-type thermocouples respectively. Thermocouple TC-1 measured the reactor temperature while thermocouple TC-2 measured the temperature on the heating jacket for feedback control. Similar thermocouples were also used to monitor temperatures on the preheating section of the setup. All the equipment were connected by ¼ inch standard Swagelok stainless steel tubing (SS-316), along with standard Swagelok ¼ inch fittings (nuts, back and front ferrules, elbows, tees, unions and end

caps). Swagelok needle valves rated at 10000 psi at 100 F were used at appropriate locations to keep sections of the setup isolated, particularly to maintain the reaction conditions inside the autoclave. Figure 5-4 shows the process diagram for the experimental setup.

Figure 5-3 Spray nozzle.

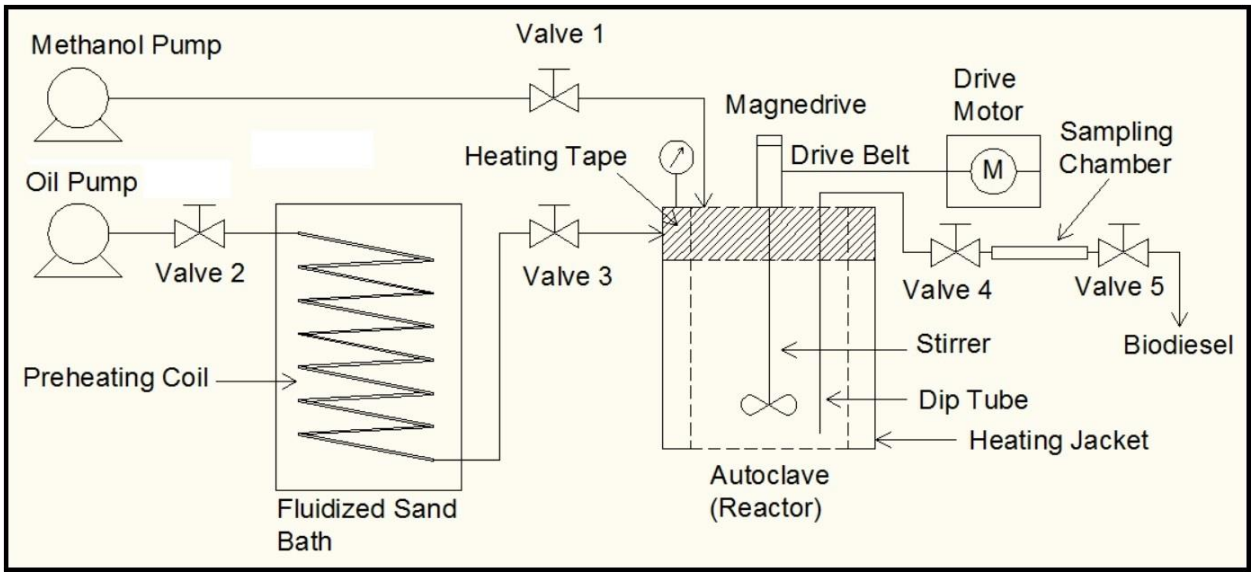

Figure 5-4 Process diagram.

5.2 Chemicals and Raw Materials

Soybean oil and methanol are the two reactants used in this experiment. Pure soybean oil (Crisco brand) was obtained from The J. M. Smucker Company and methanol was obtained from

Sigma Aldrich. The methyl heptadecanoate standard needed during the analysis was obtained from Sigma Aldrich. The sample solutions were prepared in hexane (HPLC grade), which was obtained from Fischer Scientific.

5.3 Experimental Design

For this experiment, a 2^2 factorial design with a center point replicate was implemented. The yield of methyl esters was tested against two input variables, temperature and molar ratio of methanol to oil at the respective set conditions. This being a batch process, the pressure was kept constant for all the runs, between 1700-1800 psi. Figure 5-5 represents these design variables including their combinations at low and high levels, as well as the center point.

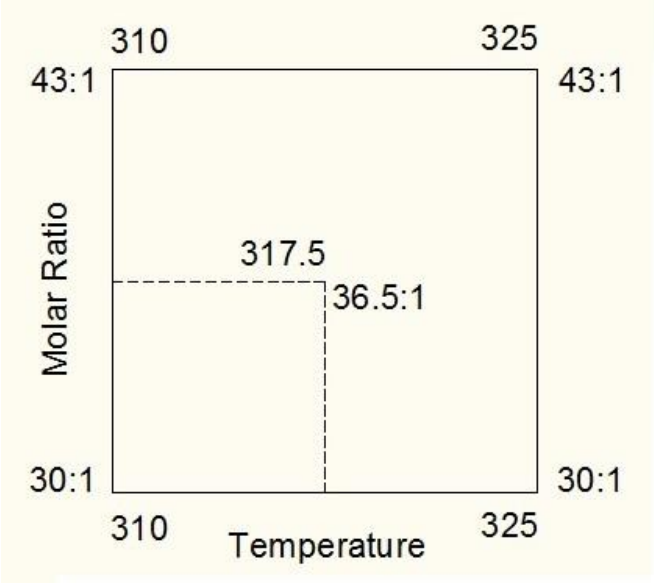

Figure 5-5 Experimental design.

Since there is more than one factor that affects the transesterification yield and it is essential to study these factors as well as their interaction, a factorial design is chosen. A 2^k (where the index k represents the number of factors or variables, 2 in this case, and the base 2 represents the levels at which each of the factors is fixed) factorial design is particularly useful since it provides the least number of experimental runs that can be used to study the k factors in a complete factorial

design [79]. Thus, a factorial design saves time due to the small sample size, and also allows to assess the interactions between the factors.

In chapter 6, the changes in output response (biodiesel yield) with respect to the changes in the factor levels (low and high for both temperature and molar ratio) are analyzed. A linear regression model is built based on the significant factors. All the experiments in the 2^2 design are run once (single replicate). Conducting an experiment that has only one run at each combination of the design conditions could be risky since there is a possibility of fitting the data against noise. In order to avoid this experimental error, a good strategy is to spread out the factor levels as apart as possible [79]. The factor levels in this design were chosen such that beyond their set values, unwanted effects were observed in the experimental output, during the preliminary testing. For example, there were effects of degradation at T > 325 °C, very poor conversion at T < 310 °C, incomplete reaction for molar ratio < 30:1 and yield saturation for molar ratio > 43:1. Thus, with a considerable difference between the low and high levels of the factors, we can obtain a reasonable estimate of the true factor effect.

One drawback associated with two-level factorial designs is the assumption of linearity. When two levels, low and high, are selected to develop a regression model, usually, the first obvious step is to try and fit a first order model. Adding the factor interaction terms to this model will allow us to anticipate the curvature of the model. But, in certain circumstances, the model may not accurately represent this curvature. Moreover, while running a two-level two factor experiment it may be more appropriate to fit a second order model [79]. In order to allow us to estimate the second order effects and give us a better prediction of the non-linearity, center points are added in replicates to the design. The addition of center points replicates allow us to get an independent estimate of the error, without affecting the error estimates of the original 2^2 design [79].

5.4 Experimental Procedure

Before the very first experiment was run, the setup was charged with nitrogen up to 2200 psi to check for any possible leakages. Since the setup was to be used at high pressures, it was essential to make sure that the setup was free of any leaks, and could withstand the operating conditions. The pumps were then set to refill mode to be charged with oil and methanol. The outlet valve of the reactor was shut and the inlet valve for methanol was opened. The methanol pump was activated and methanol was pumped into the reactor under constant flow mode. The amount of methanol was fixed for all the experiments. The amount of oil on the other hand was adjusted based on the molar ratio needed for that particular experiment.

Once the methanol was pumped into the reactor, the inlet valve was closed. The heating jacket and the heating tape were switched on, and controlled by the Autoclave Sentinel series controller and the Omega Platinum series controllers respectively. Sentinel series controller allowed for a fixed temperature set point, which was then used in a PID control mode to maintain the temperature close to the set point. Similarly the heating tape controller also allowed for a fixed set point and a PID control action. Although the Sentinel controller was able to control the temperature in auto mode, since the heating area of the jacket was significantly large, and the feedback thermocouple (TC-2) measured temperatures at a point source, there was considerable lag in the control action, and more than often the temperature would drift off away from the set point. In order to have a better control over the temperature, the controller was operated in manual mode. Figure 5-6 shows the controller face during operation.

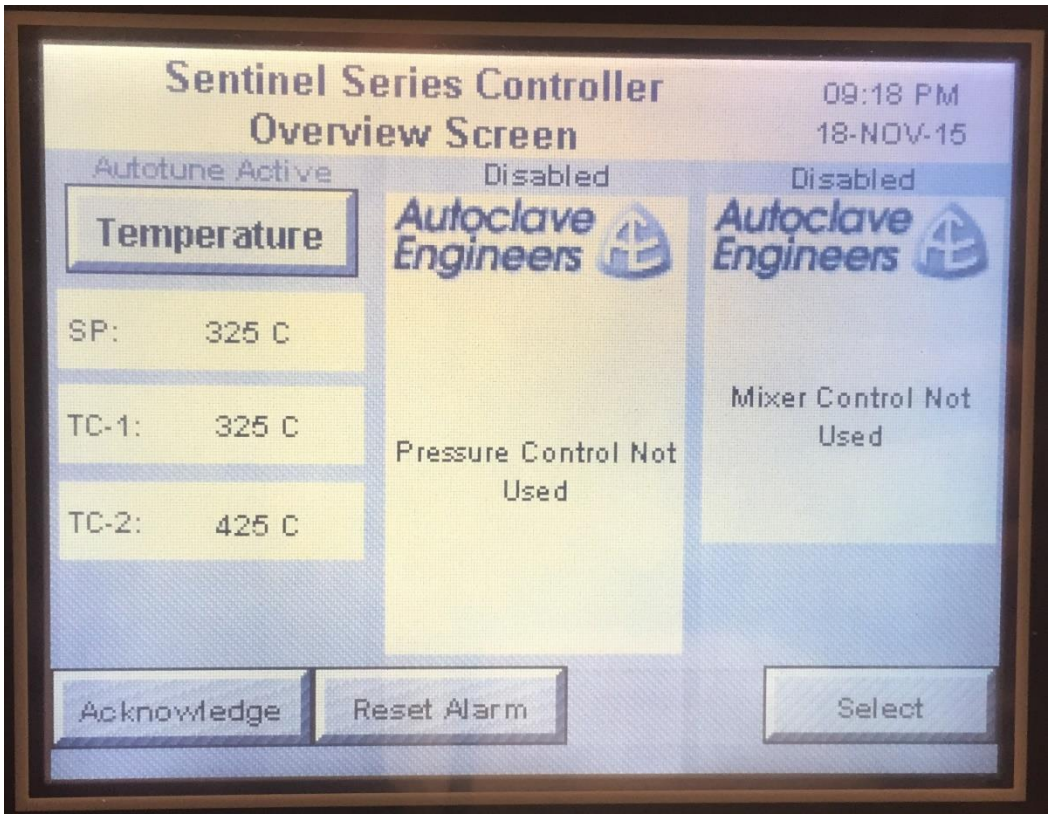

Figure 5-6 Controller screen.

The Magnedrive stirrer was switched on and set at a stirring speed of 900 rpm. The sand bath was heated to the reaction temperature. Once the autoclave temperature reached the set point, oil was pumped through the preheating coil into the autoclave, making sure that the upstream pressure was greater than the autoclave pressure to prevent back flow of methanol. This was done by adjusting the oil flow rate. The nozzle orifice was small, to allow upstream pressure buildup at high flowrates. Once the oil was pumped, the inlet valve was shut. The reaction was allowed to proceed and samples were collected at time intervals of 10 minutes each. Five samples were collected at 10, 20, 30, 40 and 50 minutes in glass test tubes and sealed with cork stoppers. For collecting the sample, the first valve in the sample isolation chamber was opened, which allowed the product to flow under pressure into the chamber. The valve was then closed and the sample was allowed to cooldown for a few minutes. The second valve was then opened and the sample

was withdrawn in a glass test tube and capped with a cork. All samples were stored in the refrigerator.

After all samples were collected, the heater and the heating tape were switched off, and the reactor was allowed to cooldown. The reactor contents were gradually withdrawn, taking care to prevent the methanol from suddenly flashing off.

5.5 Analysis of Samples

In the field of analytical chemistry, approaches using chemical methods are simpler, but there is lack of specificity and procedures tend to be time consuming. Moreover, chemical methods lack versatility and their accuracy falls off with lower concentration samples [80]. Hence, an analytical method based on an instrumental approach was used in this experimental process. Instrumental methods are faster in detection, can handle samples of complex nature and low concentration, have high sensitivities and provide reliable measurements [80].

Figure 5-7 Gas chromatograph.

The instrument used for analyzing the samples was the Agilent Technologies 7980 GC system equipped with a MTOF mass spectrometer-detector based on an ion source (Electron ion as well as Chemical ion). The GC was equipped with an Agilent HP-INNOWax column (30 m x 0.250 mm x 0.25 µm)(column 1). The GC along with the column setup are shown in figures 5-7 and 5-8 respectively.

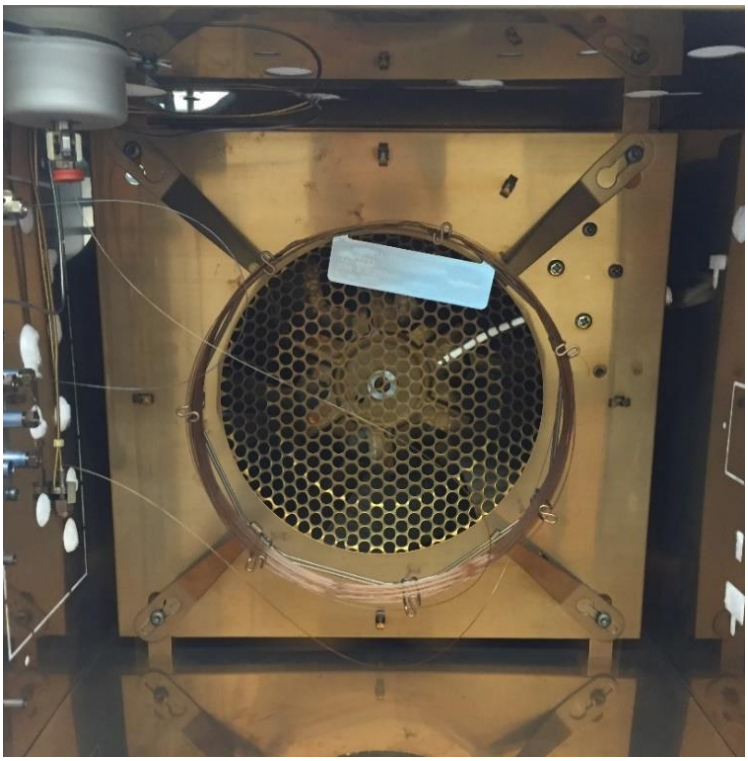

Figure 5-8 HP-INNOWax column.

The HP-INNOWax column has a polyethylene glycol (PEG) bonded and crosslinked stationary phase with high polarity and an operating temperature range of -20 to 260 °C. The column was connected to the mass detector with another column (column 2) through the EPC6. The GC is equipped with an autosampler and remotely operated by the Agilent Technologies GC-MS-QTOF software. Table 5-1 shows the column flow settings and front inlet settings for the GC. Since, the GC was operated under a constant flow mode, column pressure was not a decisive

variable. The temperature programming of the oven for both the calibration samples as well as the biodiesel samples is shown in table 5-2

Table 5-1 Front inlet and column flow settings

Parameter	Value	Unit
Front inlet temperature	250	C
Front inlet flow	49.2	mL/min
Septum purge	3	mL/min
Injection type	Splitless	-
Column 1 flow rate	1.198	mL/min
Column 2 flow rate	1.3	mL/min
Column pressure	4.98	Psi
Average velocity	319.43	cm/sec
Flow type	Constant flow mode	-

Table 5-2 Temperature programming of GC

Parameter	Rate (°C/min)	Value (°C)	Hold Time (min)	Run time
Initial	-	35	1.5	1.5
Ramp 1	15	180	0	11.167
Ramp 2	10	230	3	19.167

The analysis can be divided into two parts namely, calibration plots, and, sample preparation and quantitative analysis of samples.

5.5.2 Calibration Plots

In order to establish a relationship between the output of an instrument and actual amount of analyte present, it is essential to calibrate the instrument. Calibration involves preparing a set of solutions with a known amount of an analyte and measuring the output response of the instrument for each of these solutions. Then, a calibration plot is constructed using the output response and the known concentrations, and a relationship between the instrument response and the analyte concentration can be established. Using this relationship the instrument response of the test samples can be transformed in to the concentration of analyte present [81].

In this experiment, calibration plots were prepared using methyl heptadecanoate as the internal standard. Five samples with known concentrations in ascending order were prepared in hexane (Concentrations ranging between 50 – 375 ppm). The samples were prepared such that they covered a range of concentrations. Figure 5-9 shows the overlaid chromatograms for methyl heptadecanoate samples.

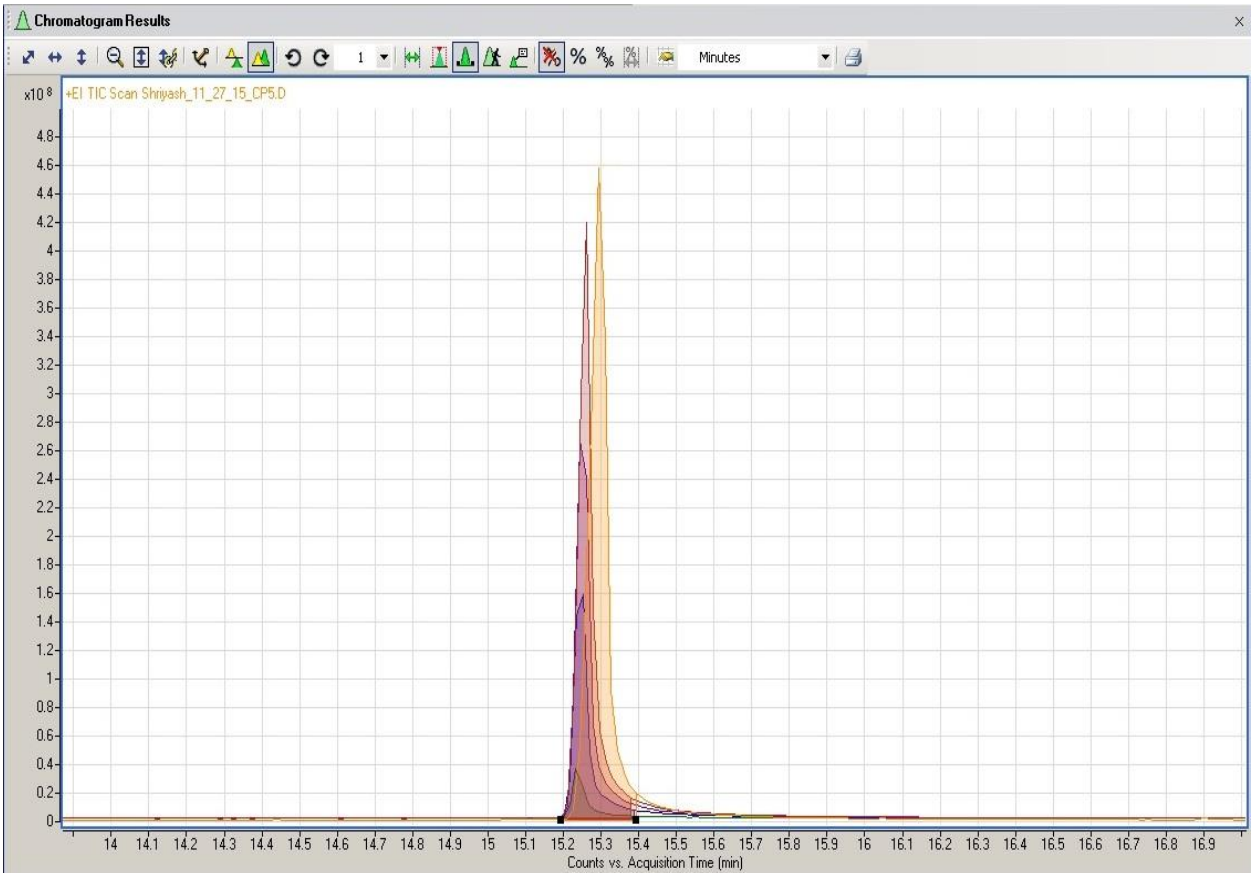

Figure 5-9 Chromatograms for the calibration standard.

The peak areas were calculated by integrating the peaks using the Agilent Qualitative Analysis of Mass Hunter Acquisition Data software. The software allowed for automatic integration of peaks, as close to the baseline as possible. Smaller peaks were manually integrated. The peak areas were plotted against the known concentrations and a calibration plot was generated as shown in figure 5-10.

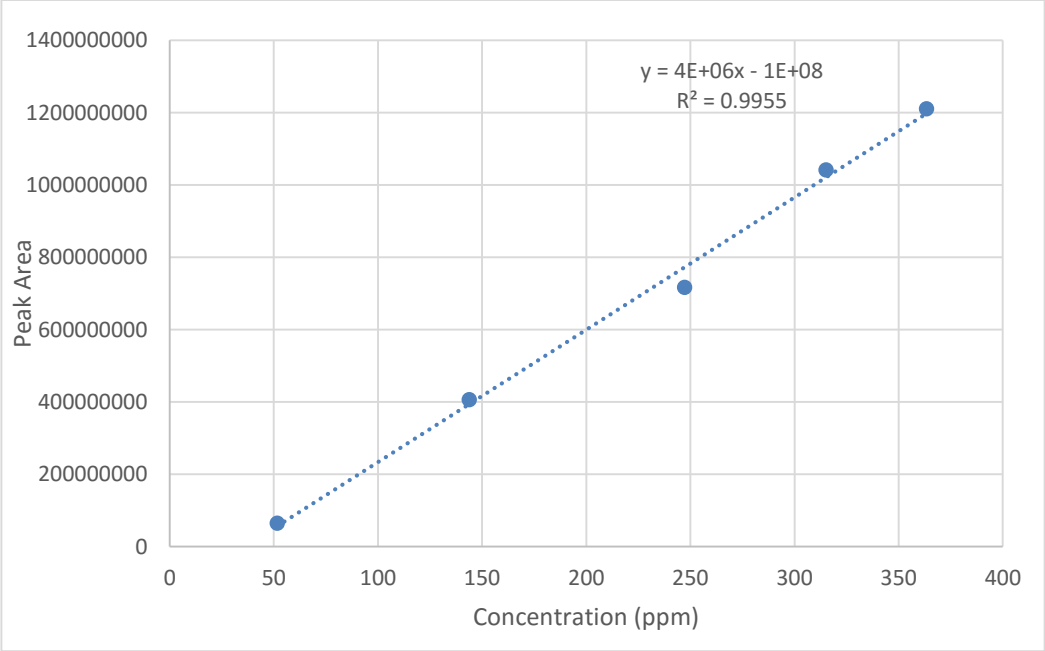

Figure 5-10 Calibration plot for methyl heptadecanoate internal standard.

The equation of the trendline represents the relationship between the instrument response and the concentration of analyte present. This equation was used as the basis to convert all the peak areas to their respective concentrations in the quantitative analysis of the biodiesel samples. A coefficient of determination (R^2) value close to 1 indicates that there is a strong correlation between the peak areas detected by the GC and the concentrations prepared.

5.5.3 Sample Preparation and Quantitative Analysis

The main objective in analyzing the samples was to determine the ester (FAME) content in the biodiesel and thereby calculate the yield for each point in the factorial design, at reaction times 10, 20, 30, 40, and 50 minutes. The biodiesel samples were collected and stored in glass test tubes at about 8 °C in the refrigerator, away from light and heat. The samples were allowed to settle for about 24 hours to separate into three distinct phases of unreacted (excess) methanol, biodiesel and glycerol, as seen in the figure 5-11.

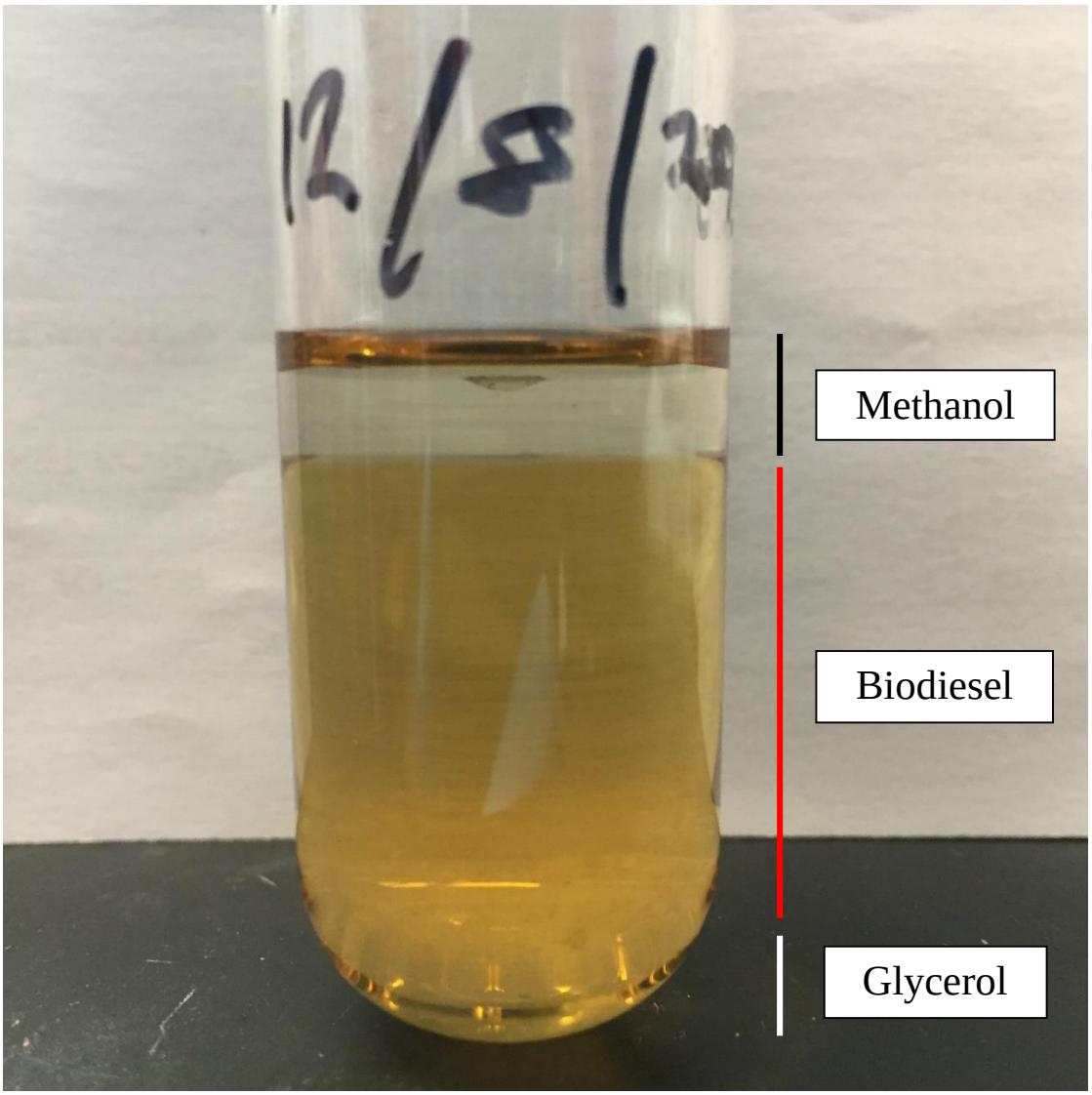

Figure 5-11 Collected sample and phases after 24 hour disengagement period.

A similar sample preparation procedure was followed for all the samples collected at 10, 20, 30, 40 and 50 minute time intervals. About 2 mL of biodiesel was carefully drawn out with a syringe, without disturbing the other phases of methanol and glycerol. The sample was then introduced in a 4 mL glass vial and capped. Although, most of the methanol was separated from the biodiesel phase during the 24-hour settling period, a small amount of methanol was thought to be mixed with the biodiesel phase and likely drawn out along with it in the glass vial. In order to completely separate out the methanol, the vials were kept in a freezer at –20 °C for about 30 minutes. This

allowed the samples to freeze completely. The vials were then removed from the freezer and brought to the ambient temperature. Since the melting point of methanol is lower than biodiesel, two distinct phases, one of pure biodiesel and the other of methanol, formed with gradual increase in the temperature.

A small amount of biodiesel was drawn out with a clean glass syringe and dispersed in a 20 mL scintillation vial. It was then further diluted to about 1000 parts per million with hexane, to form the B100 stock solution (100% biodiesel). The scintillation vials were held in a sonicated water bath for about 30 seconds to make sure that the solution was well mixed. Using this stock solution, two GC samples were prepared in 2 mL GC vials and diluted with hexane such that their concentrations were approximately in the center of the range of the calibration plot. The samples were then spiked with a known amount of the internal standard. Preparing two dilute samples (replicates) of similar concentrations was essential in establishing the precision as well as the accuracy of the method. Similar samples were prepared for each of the 10, 20, 30, 40 and 50 minute samples.

The sample vials were then placed into the autosampler tray of the GC. The sequence and temperature programming method were loaded in the software. Based on the sequence, the autosampler draws each sample and injects in to the GC column through the front inlet. The sample is then subjected to the temperature programming while it runs through the column under the set column flow. Figure 5-12 shows the chromatogram of one of the biodiesel samples. The chromatogram was then analyzed both quantitatively and qualitatively.

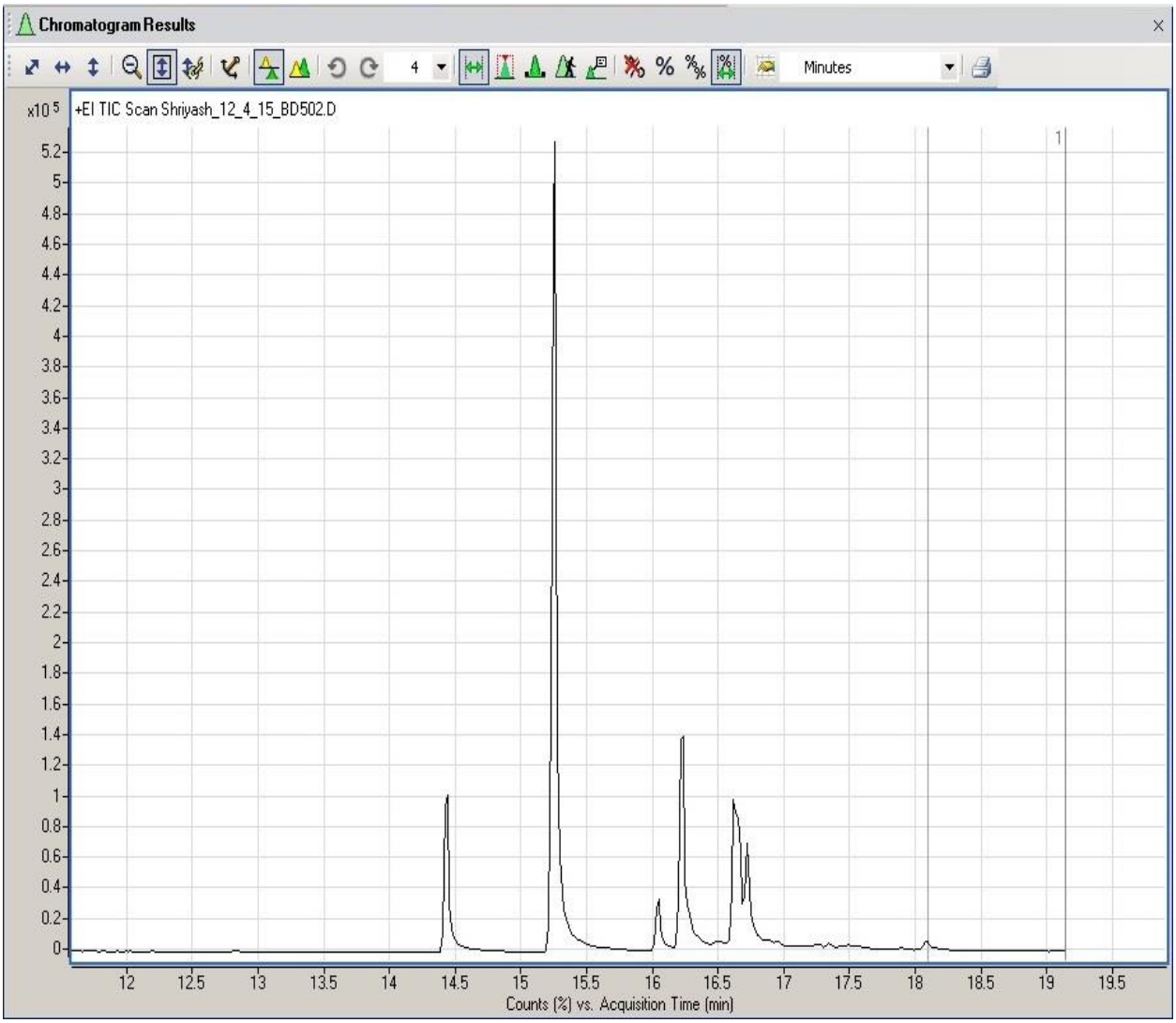

Figure 5-12 Biodiesel chromatogram.

5.6 Analysis Results

The next step after acquiring the chromatograms of the biodiesel samples, was to integrate and find the areas under the peaks. The software allowed for automatic integration of the peaks. Smaller peaks that could not be recognized with the software, were manually integrated. To reduce the error associated with manual integration, it was done by following the baseline. Figure 5-13 shows the integrated peaks for the methyl esters.

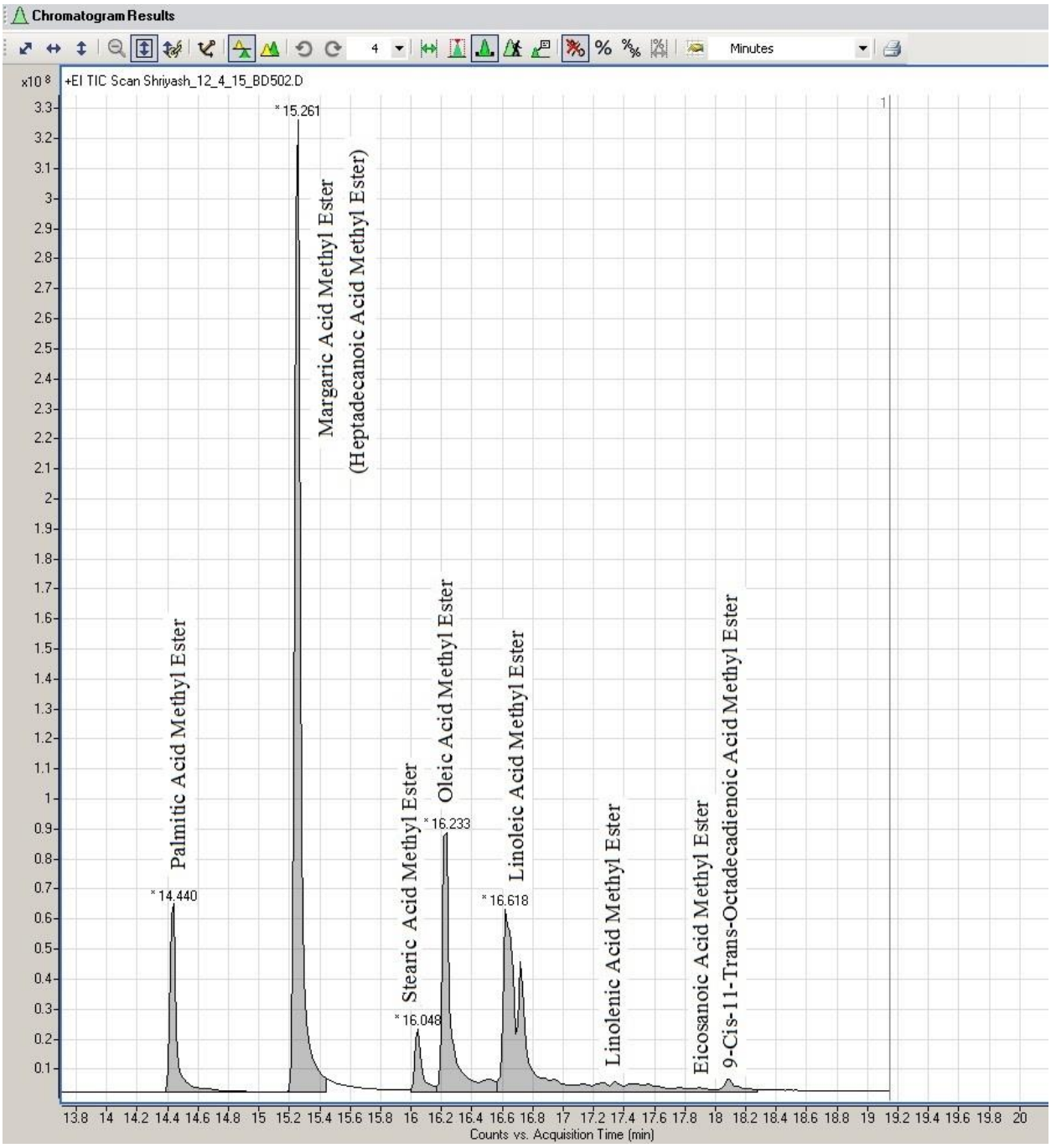

Figure 5-13 Integrated methyl ester peaks.

Seven different methyl esters were obtained from the sample along with the margaric acid methyl ester internal standard (heptadecanoic acid methyl ester). As seen in the chromatogram, palmitic acid methyl ester, stearic acid methyl ester, oleic acid methyl ester and linoleic acid methyl ester were the significant ones. The other methyl esters present were linolenic acid methyl ester,

eicosanoic acid methyl ester and 9-cis-11-trans-octadecadienoic acid methyl ester. The relative size of the peaks and the electron ionization spectra for each of these methyl esters are shown in appendix B.

Once the peak areas were obtained, the concentration of each methyl ester was calculated using the equation of the trendline of the calibration plot. The total concentration was obtained from the sum of the individual concentrations of the methyl esters. The biodiesel yield was then calculated by multiplying the ratio of calculated concentration to the prepared concentration of samples by 100. A sample calculation is shown in appendix C. For each experiment in the design, and for each residence time from 10 to 50 minutes, the yields were calculated. The table 5-3 gives the yields for each of the reaction conditions at all reaction times.

Table 5-3 Yield data

Time (min)	Yield (%)					
10	90.05	85.57	78.04	75.05	78.83	79.79
20	94.00	89.35	84.21	80.91	84.39	84.49
30	96.36	92.27	86.34	83.32	87.43	87.56
40	97.06	94.17	87.01	83.46	90.01	90.24
50	97.26	94.95	87.44	83.47	91.83	92.30
Temperature (°C)	325	310	325	310	317.5	317.5
Molar ratio	43	43	30	30	36.5	36.5

The center point data was averaged and a yield vs time plot was generated as shown in figure 5-14. The figure shows how the yield increases over time at different reaction conditions.

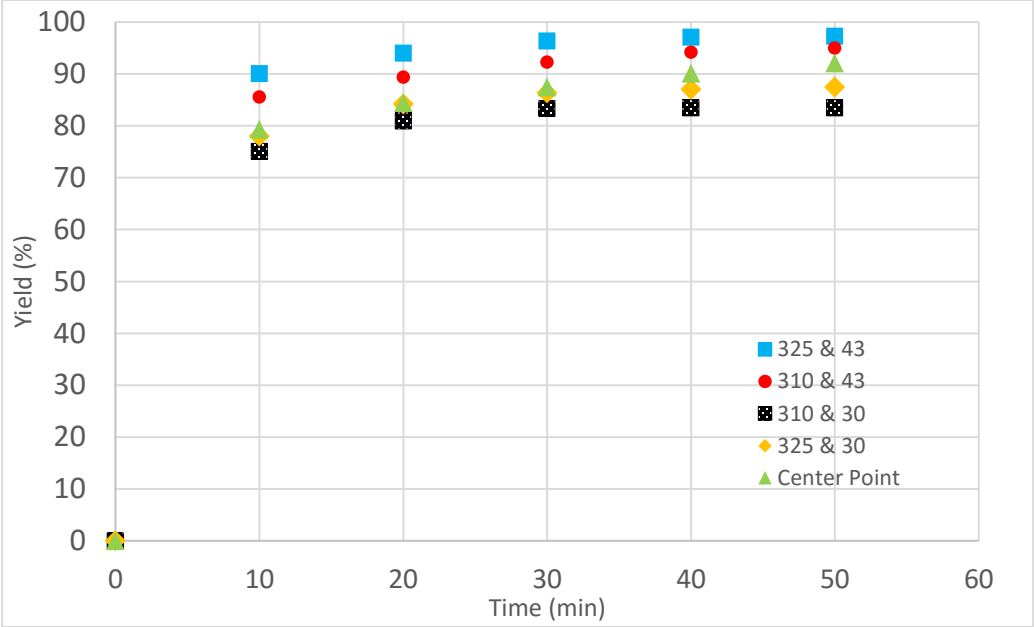

Figure 5-14 Yield versus Time plot for biodiesel samples (center point at 317.5 °C and 36.5 molar ratio).

Similar yield versus time plots were generated for each of the reaction conditions. The figures 5-15, 5-16, 5-17, 5-18 and 5-19 show these plots with error bars at 5% uncertainty (or 95% confidence level).

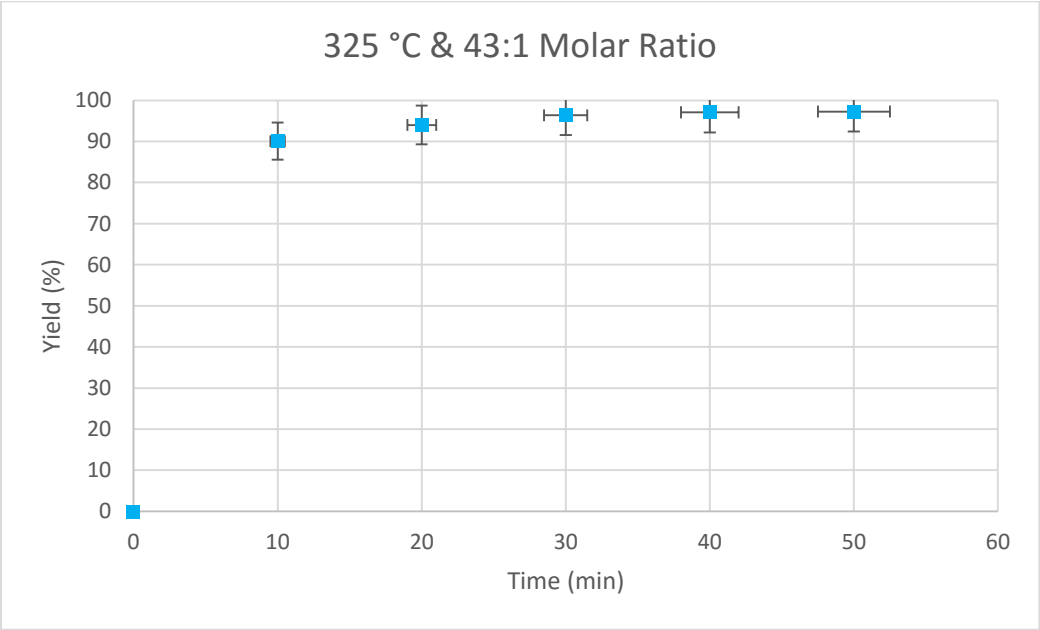

Figure 5-15 Yield vs Time plot for 325 °C and 43:1 molar ratio.

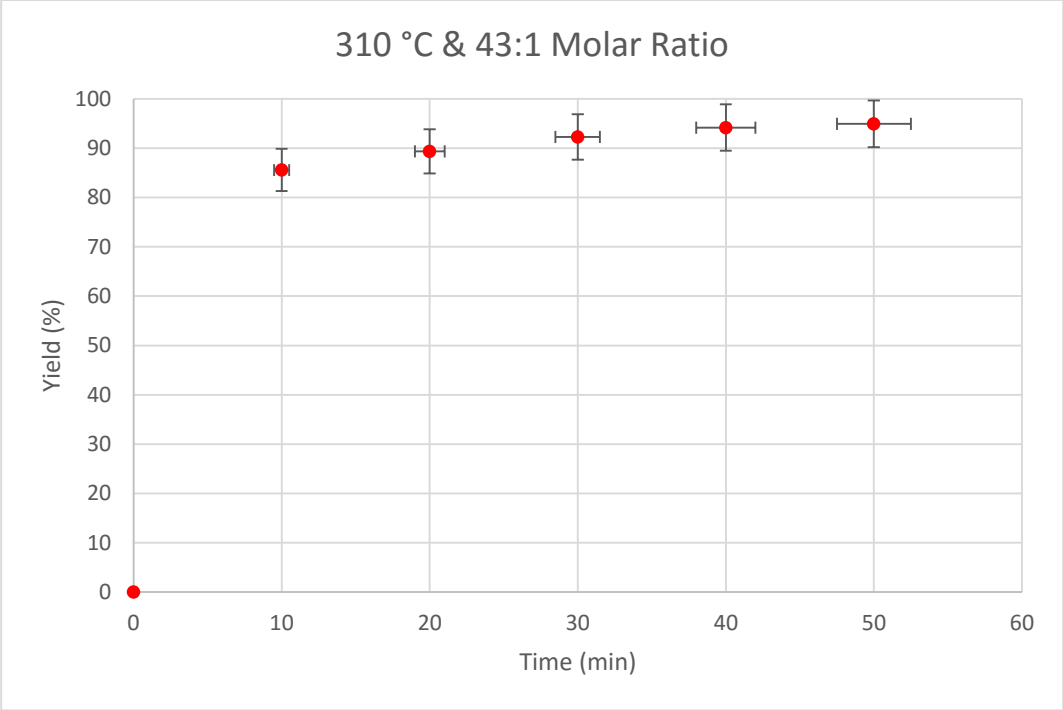

Figure 5-16 Yield vs Time plot for 310 °C and 43:1 molar ratio.

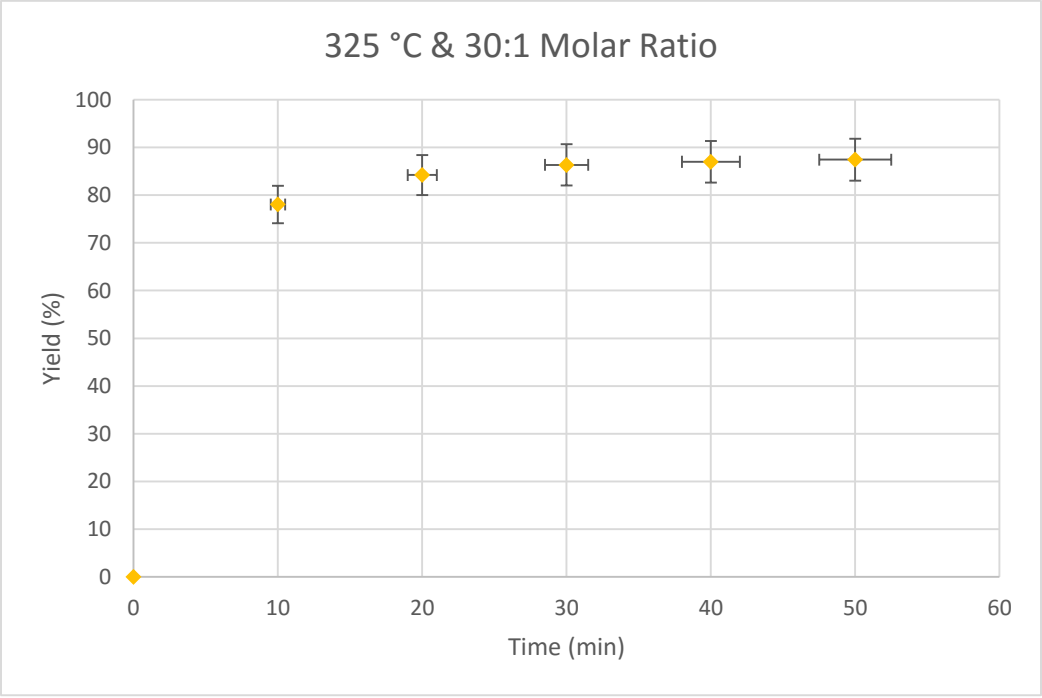

Figure 5-17 Yield vs Time plot for 325 °C and 30:1 molar ratio.

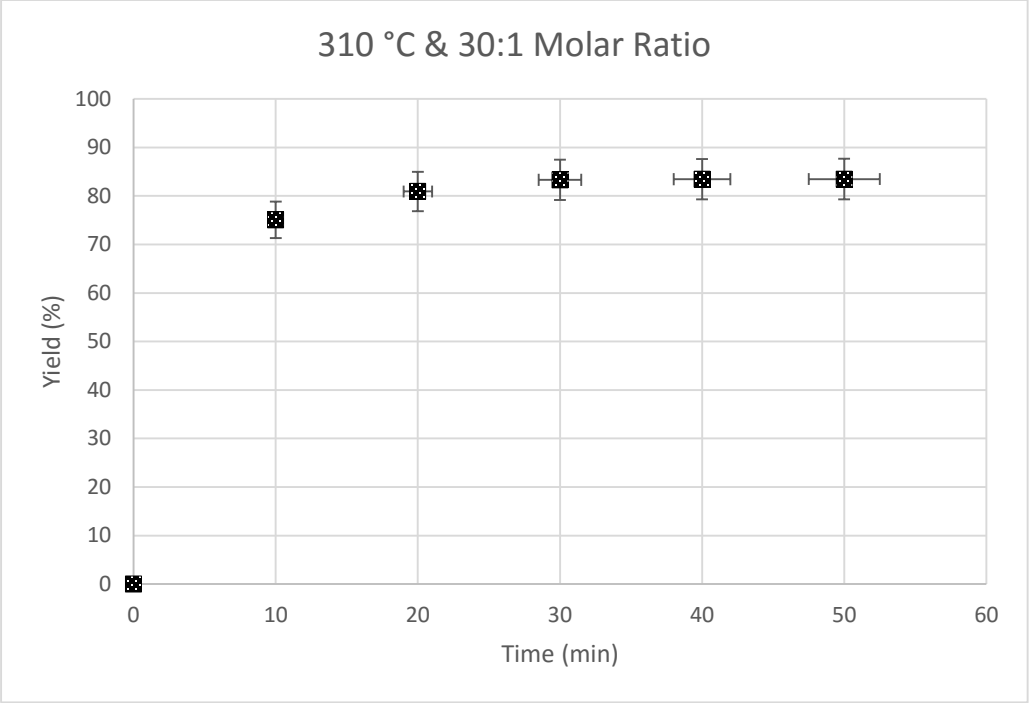

Figure 5-18 Yield vs Time plot for 310 °C and 30:1 molar ratio.

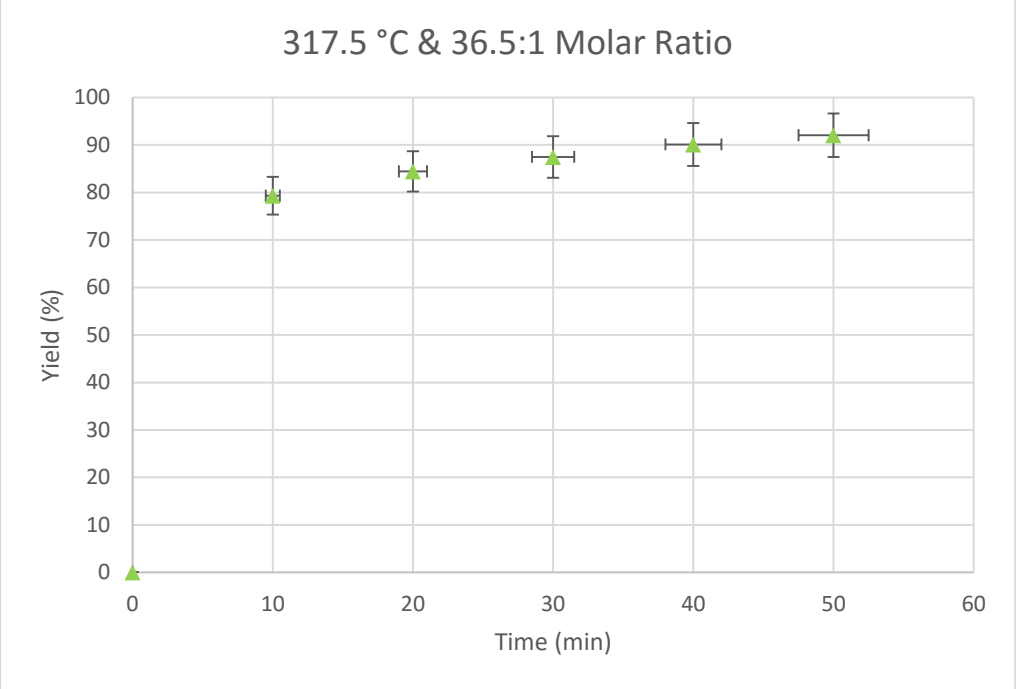

Figure 5-19 Yield vs Time plot for 317.5 °C and 36.5:1 molar ratio (center point).

CHAPTER 6: ANALYSIS OF VARIANCE (ANOVA) AND DEVELOPMENT OF REGRESSION EQUATION

The experimental design chosen here is a 2^2 factorial design with a single replicate and with added center points. In a two-level factorial design like this, we can define the factor effects and the interaction effects. The factor effects can be defined as the change in output produced due to the change in the level of one factor. It is important to note that this change is averaged over the levels of the other factor. The interaction effect can be defined as the average difference between the effect of one factor at the highest and at the lowest levels of the other factor [79]. In this design, there are two main factor effects and one interaction effect. Variance analysis methods have been used to determine the significance of the factors, temperature and molar ratio, as well as the significance of the interaction between temperature and molar ratio.

Analysis of variance involves treating the output of the experiment (yield in this case) as a random variable. The output is based on the factor levels that need to be compared. Before generating the analysis of variance table, we need to convert the design factors from their natural engineering units to coded design variables. This implies changing the numeric values of the design factors to $-1 \leq x_i \leq +1$, where x_i is the design factor. Coding the variables has many advantages. By coding the variables, it is possible to compare the magnitudes of the model coefficients directly. Coding the variables makes them dimensionless, further, the effect of changing each design factor over one unit interval can be measured. Moreover, the model coefficients are estimated with the same precision. Coded variables also help in determining the

relative size of the factor effects [79]. Coded variables can be obtained using the equation shown below:

$$Coded\ Value = \frac{Actual\ value - Mean\ of\ the\ range}{\left(\frac{Difference\ in\ range}{2}\right)} \quad (6.1)$$

The calculations to obtain the coded variables are shown in appendix C. The coded variables obtained with this equation are shown in the table 6-1.

Table 6-1 Coded values

Temperature	**Level**	**Numeric Value**	**Coded Value**
	Low	310 ℃	-1
	High	325 ℃	+1
Molar Ratio	**Level**	**Numeric Value**	**Coded Value**
	Low	30	-1
	High	43	+1

Once the coded variables are obtained, the analysis of variance table can be built, using which we can find the contrasts, the effects and the sum of squares, degrees of freedom and the mean square for the treatments. We also need to find the total sum of squares, the degrees of freedom for the error and the mean square error. The objective of this exercise is to find the significant factors and interactions, using which we can build a regression equation that relates them to the biodiesel yield. The 50 min reaction sample was chosen as the defining sample, since the yields are maximum for all reaction conditions at 50 minutes. The analysis of variance table for at 50 minutes of reaction time is shown below.

Table 6-2 Analysis of variance (ANOVA)

Treatment	**Main Factors**		**Interaction**	**Output**
	T	***MR***	***T*MR***	***Yield (50 min)***
Both Low	-1	-1	1	83.46203
Molar Ratio (MR) high	-1	1	-1	94.17916
Temperature (T) high	1	-1	-1	87.01097
Both high	1	1	1	97.06953

Using this data and the calculations mentioned above, the mean squares were calculated. An F-test was performed at 95% confidence level to find out if the main factors and the interaction were significant. Only molar ratio passed the F-test while temperature and the interaction failed the F-test. In other words, the F_0 was greater than $F_{critical}$ for molar ratio, thus making it the only significant factor. This was verified by calculating the p-values for temperature, molar ratio and their interaction. The detailed calculations are shown in appendix C, while the table 6-3 lists the p-values as well as the values from the F-test for the two main factors and the interaction.

Table 6-3 P-values for the factors and interactions

Factor	**P-value**	**F_0**	**$F_{critical}$**	**Significance**
Temperature	0.305005	1.868611	18.51282	No
Molar Ratio	0.043397	21.554332		Yes
Interaction	0.751716	0.131389		No

The regression model obtained from the regression coefficients is,

$$Yield = 90.78 + 5.32 * (Molar\ Ratio) \quad (6.2)$$

The curvature (non-linearity) of the model was tested and it was found that the assumption of linearity was correct. The non-linearity of the model is insignificant. The results are shown in table 6-4.

Table 6-4 Test for curvature

Yield	y_1	y_2
	91.83162	92.29717
y_c	92.06439	
y_i-y_c	-0.23277	0.23277
y_f	90.78349	
$SS_{Pure\ quadratic}$	2.187614	
df	1	
$MS_{Pure\ quadratic}$	2.187614	
MS_E	0.108367	
F_0 for pure quadratic	20.18707	
$F_{critical}$	161.4476	
p-value	0.139419	
Significance of quadratic assumption	No	

To check for significant factors at other reaction times, similar calculations were also performed. Even at these reaction times, it was found that molar ratio is the only factor which affects the yield more significantly. The p-values and regression models for all reaction times are listed in the table 6-5.

Table 6-5 P-values and regression models

Time (min)	P-values			Regression Model
	Temperature	Molar Ratio	Interaction	
10	0.245073	0.039082	0.776759	Yield = 82.18 + 5.63*MR
20	0.225392	0.057895	0.796154	Yield = 87.12 + 4.55*MR
30	0.261375	0.053870	0.839138	Yield = 89.57 + 4.74*MR
40	0.295763	0.045511	0.899069	Yield = 90.43 + 5.19*MR
50	0.305005	0.043397	0.751716	Yield = 90.78 + 5.32*MR

6.1 Surface Plots

The results obtained from the analysis of variance can be further verified by the surface plots for yield versus temperature and yield versus molar ratio. As seen in figure 6-1, the change in yield is fairly linear with the change in molar ratio at all reaction times. On the other hand, the change in yield with respect to the change in temperature depends on the molar ratio used at those particular temperatures. In figure 6-2, despite the temperature being lower, the yield is higher where the molar ratio used was 43:1, and lower where molar ratio used was 30:1. In other words, this confirms the significance of molar ratio being much higher than that of temperature.

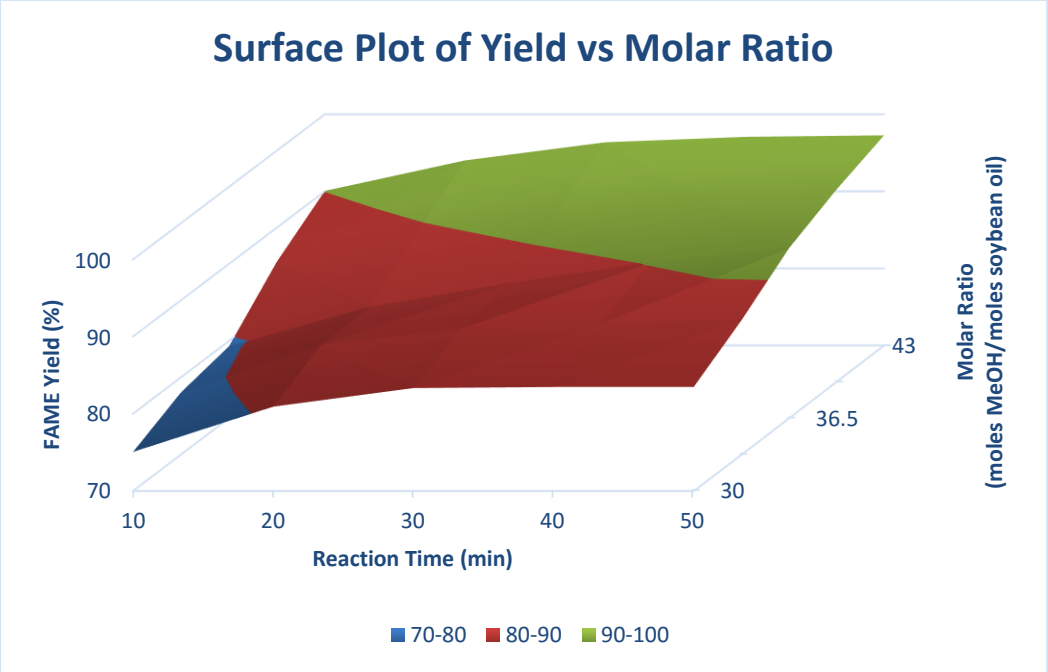

Figure 6-1 Surface plot of Yield vs Molar Ratio

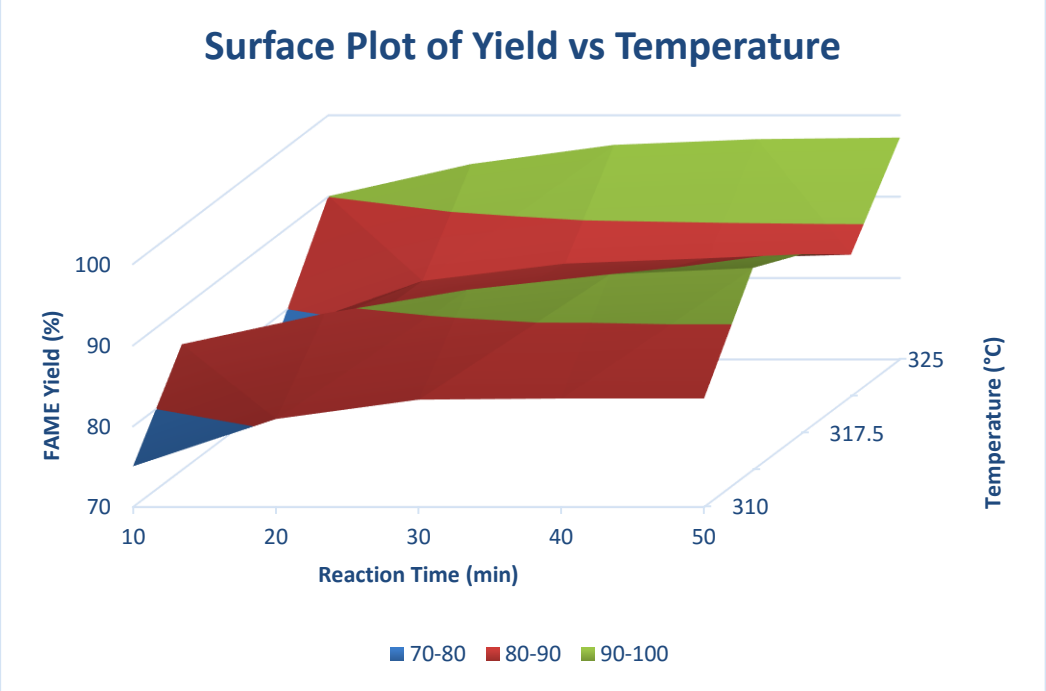

Figure 6-2 Surface plot of Yield vs Temperature

6.2 Residual Analysis

Using the regression equation of the model and the coded variables at the design conditions, the model based yields are calculated. The difference in the actual yields and the model based yields gives the residuals. A normality plot can be then generated for the residuals to check the error distribution. The normality plot for the residuals is shown in figure 6-3.

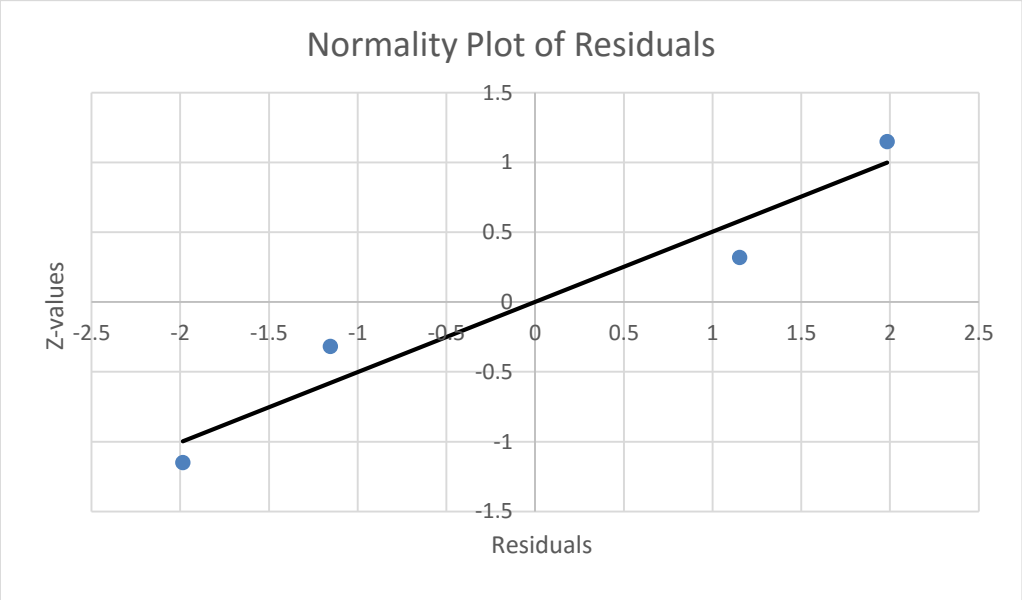

Figure 6-3 Normality plot of residuals.

As seen in the figure, the errors are normally distributed without any departure from normality. This implies that the model assumptions have been satisfied.

CHAPTER 7: A SIMPLE LUMPED TENDENCY MODEL FOR TRANSESTERIFICATION

This chapter briefly describes the preliminary study to determine the kinetic tendency of the reaction. Based on the integral method, a kinetic equation was obtained for the first order reversible reaction. Using this equation the rate constants were predicted based on a non-linear regression approach. The Arrhenius plot was generated for the rate constants and the values of activation energy and pre-exponential factor were determined.

7.1 Kinetic Tendency of the Reaction and Estimation of Rate Constants

Using the collected experimental data, a preliminary study was performed to determine the kinetic tendency of the supercritical transesterification reaction. Although at high molar ratios, the reverse reaction can be ignored, for the purpose of estimating the kinetic tendency the effect of the reverse reaction is taken into account. Thus, for kinetic purposes, the reaction is assumed to follow first order reversible rate-law as a function of triglyceride concentration. Assuming the supercritical transesterification reaction to follow the first order reversible rate law, the rate constants were estimated.

For a first order reversible reaction,

$$r_A = k_f C_A - k_b C_B = -\frac{dC_A}{dt} \tag{7.1}$$

At t = 0, $C_A = C_{Ao}$ and $C_B = 0$, then equation (7.1) can be integrated as follows

$$-\int_{C_{A_0}}^{C_A} \frac{dC_A}{k_f C_A - k_b (C_{Ao} - C_A)} = \int_0^t dt \tag{7.2}$$

$$\frac{1}{k_f + k_b}\left\{ln\left[k_f C_A - k_b(C_{Ao} - C_A)\right] - ln\left(k_f C_{Ao}\right)\right\} = -t \tag{7.3}$$

$$\frac{k_f C_A - k_b C_{Ao} + k_b C_A}{k_f C_{Ao}} = e^{-(k_f + k_b)t} \tag{7.4}$$

$$C_A(k_f + k_b) = k_b C_{Ao} + k_f C_{Ao} e^{-(k_f + k_b)t} \tag{7.5}$$

$$C_A(k_f + k_b) = k_b C_{Ao} + k_f C_{Ao} - k_f C_{Ao} + k_f C_{Ao} e^{-(k_f + k_b)t} \tag{7.6}$$

Solving for C_A,

$$C_A = C_{Ao}\left[1 - \frac{k_f}{k_f + k_b}(1 - e^{-(k_f + k_b)t})\right] \tag{7.7}$$

Reactant concentration can be represented in terms of conversion as,

$$C_A = C_{A_0}(1 - x)$$

Substituting for C_A in equation 7.7,

$$x = \frac{k_f}{k_f + k_b}(1 - e^{-(k_f + k_b)t}) \tag{7.8}$$

where,

k_f is the rate constant for the forward reaction and k_b is the rate constant for the backward reaction.

Equation (7.8) gives the kinetic expression in terms of conversion. Since we have the experimental results in terms of biodiesel yield, they need to be converted into conversion of the reaction. The transesterification reaction conversion can be expressed as a ratio of methyl ester weight percent (biodiesel yield) to the initial weight percent of triglycerides. Since we are using pure soybean oil, the weight percent of triglycerides can be considered 99.9 %. Thus, from the experimental data, the conversion corresponding to each reaction condition at each time step was

calculated. Once the conversion-time data is known, using the proposed rate equation, the specific rate constants can be determined.

A non-linear data fitting approach was then employed to fit the model to the data and determine the rate constants. Based on the assumed model, conversion was calculated for an initial guess of 'k_f' and 'k_b' using equation (7.8). The generalized reduced gradient (GRG) algorithm was applied with the Excel solver to perform non-linear regression. The objective was to minimize the sum of squares of the differences between the conversion determined experimentally and that predicted using the model for the initial values, by iterating the values of k_f and k_b, subject to the constraints $k_f > 0$ and $k_b > 0$. The k values are shown in the table below.

Table 7-1 Rate constants determined with non-linear regression

Reaction Conditions		k_f (min^{-1})	k_f (sec^{-1})	k_b (min^{-1})	k_b (sec^{-1})
Temperature (°C)	Molar Ratio				
325	43:1	0.24916	0.00415	0.00653	0.00011
310	43:1	0.22902	0.00382	0.01698	0.00028
317.5	36.5:1	0.21006	0.00350	0.02398	0.00040
325	30:1	0.20183	0.00336	0.03045	0.00051
310	30:1	0.19971	0.00333	0.03880	0.00065

The plots for the experimental and predicted values are shown in figures 7-1 and 7-2. The values of rate constants obtained by this method are in close agreement with those obtained by Saka and Kusdiana in their work. As observed in the plots, the experimental conversion reaches a plateau after about 30 minutes of reaction time. This suggests that the reaction reaches an equilibrium state, where no more product can be formed. In other words, the reaction is equilibrium limited at longer residence times. The values of the rate constants corresponding to the forward and backward reactions are shown in table 7-1. It can be observed that the values of k_f are much higher than the values of k_b. This suggests that the forward reaction is dominating and that the

excess methanol does drive the reaction towards the formation of methyl esters. Thus, the effect of the reverse reaction is very small, particularly at higher temperature and higher molar ratio.

There might be a possibility of the dependence of the reaction order on the intermediates (diglycerides and monoglycerides). Since the determination of concentrations of the intermediates was beyond the scope of this work, kinetic studies to check for other reaction orders were not performed. This work was thus limited up to determining the kinetic tendency of the reaction.

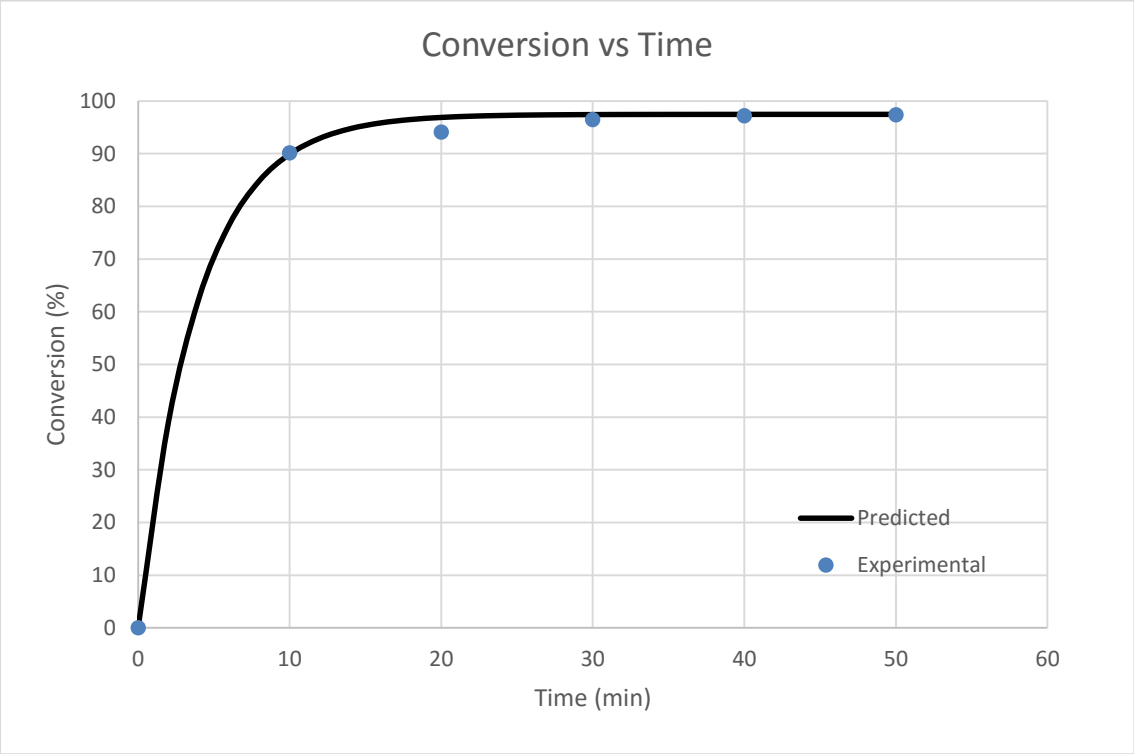

Figure 7-1 Experimental and predicted data at 325 °C and 43:1 molar ratio.

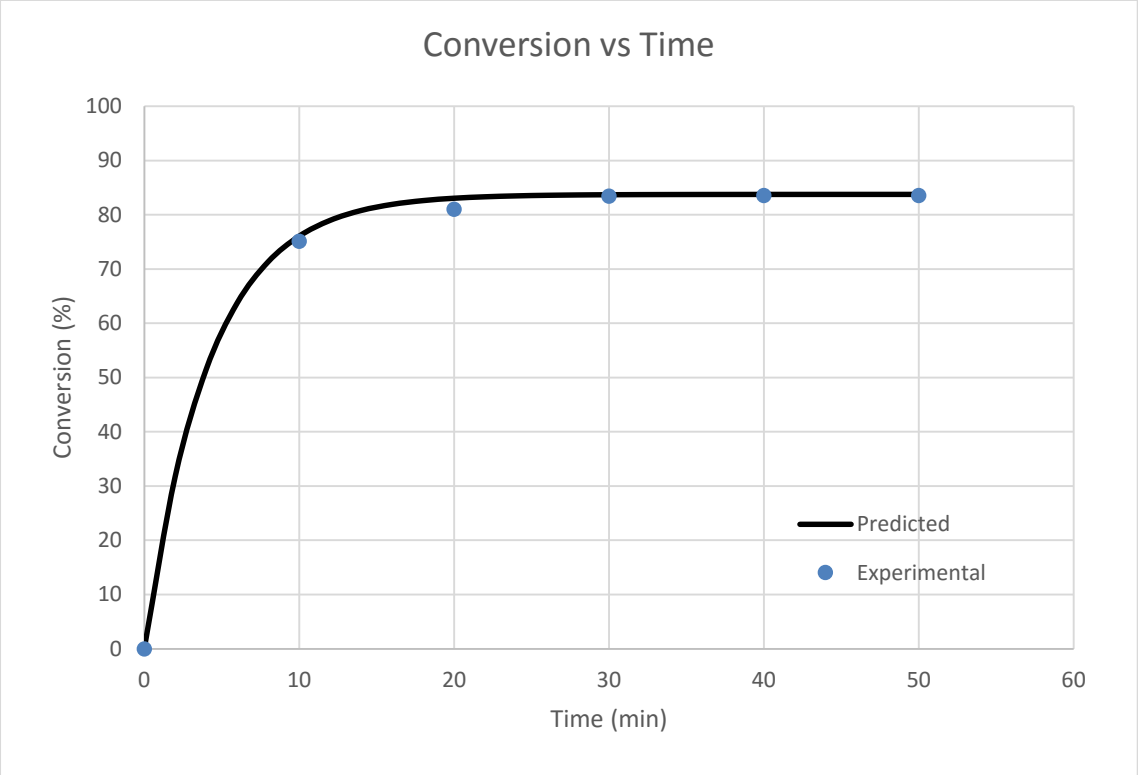

Figure 7-2 Experimental and model data at 310 °C and 30:1 molar ratio.

7.2 Arrhenius Plot and Activation Energy

The Arrhenius equation can be used to correlate the temperature dependence of the rate constants [82]. Using the rate constant values obtained from the non-linear regression, an Arrhenius plot can be generated to determine the activation energy for the reaction. The Arrhenius equation in exponential form is:

$$\mathrm{k} = \mathrm{A}e^{\frac{-E_a}{RT}} \tag{7.9}$$

where,

k is the rate constant; A is the pre-exponential factor; E_a is the activation energy; R is the gas constant (8.314 J mol^{-1} K^{-1}) and T is temperature in Kelvin.

The Arrhenius equation can be linearized as:

$$\ln(k) = \ln(A) - \frac{E_a}{RT} \tag{7.10}$$

Using the temperature-rate constant data for the forward reaction, $\ln(k_f)$ can be plotted against (1/T) and the activation energy can be found using this graph. The calculations are shown in appendix C. The Arrhenius plot for the forward reaction is as shown in figure 7-3. The values for activation energy and pre-exponential factors are tabulated in table 7-2.

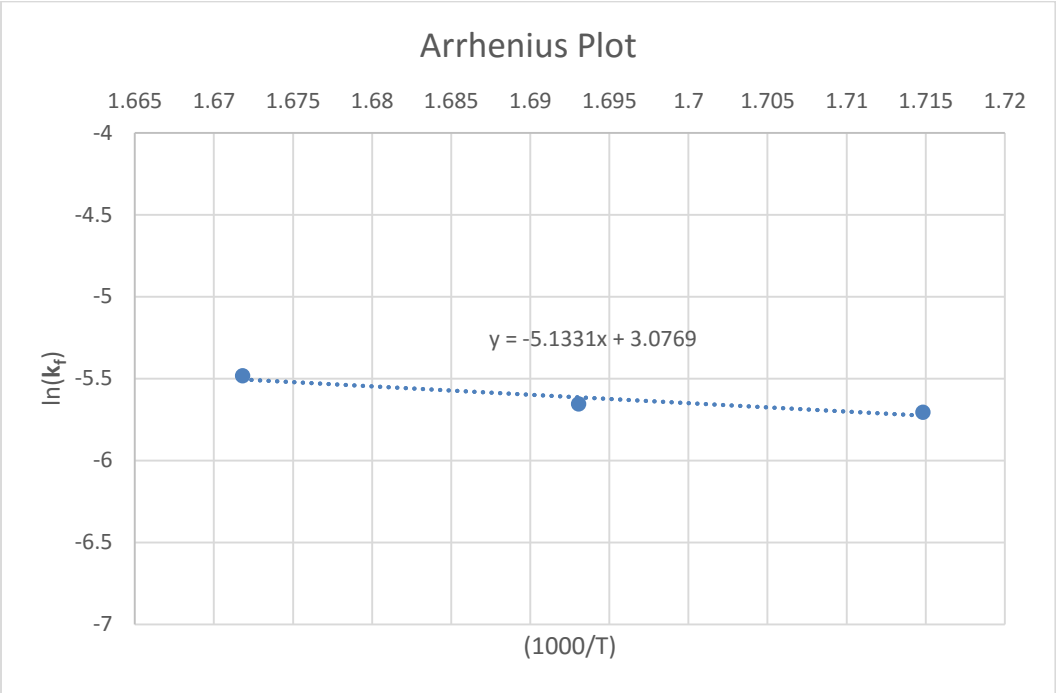

Figure 7-3 Arrhenius plot for forward reaction.

Table 7-2 Activation energy and pre-exponential factor for the forward reaction

Activation Energy (E_a) (kJ/mol)	Pre-exponential Factor (A)
42.676	21.691

CHAPTER 8: CONCLUSIONS AND RECOMMENDATIONS

The production of biodiesel under supercritical conditions was studied in a batch reactor. Biodiesel was produced from soybean oil through transesterification with methanol at supercritical conditions. Past research has proved that transesterification using supercritical fluids has several advantages over conventional transesterification methods. This study was conducted using a pilot scale experimental system which is scalable to a continuous operation. Milder operating pressures than those presented in earlier studies were used. This chapter is aimed at providing the conclusions of this research as well as recommendations to enhance the intrinsic merits of this study.

8.1 Conclusions

The work presented a methodology to produce biodiesel from transesterification of vegetable oils using supercritical methanol. This study included the method development for analyzing the biodiesel samples using a gas chromatograph. Biodiesel yields were determined using gas chromatography and the effects of the key reaction variables like molar ratio and temperature on yield were studied. Variance analysis was carried out to determine which factor(s) and factor interactions significantly affect biodiesel yield. It was found that molar ratio has the strongest effect on biodiesel yield. Although the reaction yield depends on temperature as well, this dependence was observed to be far weaker as compared to that on molar ratio. Using linear regression, a regression model was developed which relates the molar ratio and the biodiesel yield.

A preliminary kinetic study was performed to determine the rate constants of the transesterification reaction under supercritical conditions. The reaction was assumed to be first order reversible and the rate constants were determined by non-linear regression. The values of

rate constants suggest that the forward reaction is dominating and that the effect of the reverse reaction is negligible. The data predicted by the model and that obtained experimentally is in close agreement. From the experimental data, it can be observed that the reaction conversion approaches a steady state at longer residence times. This suggests that the reaction is equilibrium limited, particularly at long residence times.

Significant work has been done in the past on biodiesel production using supercritical technology, particularly the work done by Saka and Kusdiana (2001), and He et al. (2007), is notable. Although this thesis presents the work on a similar technology for biodiesel production, the reactor used in this work is 1 liter in volume, as opposed to the 5 ml to 200 ml reaction vessels used in the studies before. Thus, the scale of the reactor used here is significantly larger as compared to that in any of the past work. From a perspective of the kinetic study, the reactor used here is by far the largest reactor used till date. Further, the batch type setup used here can be easily converted to a continuous mode thereby allowing a much higher production capacity. These key differences in the equipment represent the true scalability of this technology. The pressures used here were within 11-13 MPa range as opposed to the 28 MPa to 65 MPa pressures used in the past. Although the pressures used in this work are much milder (but within the supercritical region) in comparison with the past work, the yields are comparable and still within the 90% plus range. Thus, it can be seen that supercritical transesterification can give promising results even at milder conditions.

8.2 Recommendations and Future Work

Each experiment in the factorial design was performed once, with the exception of the center point. In other words, the factorial design involved one replicate ($n=1$) experiments. One replicate experiments were chosen to maintain a balance between the time consuming nature of the experiment and the time constraints associated with the completion of this project. The choice

of this sample size plays a significant role in controlling the type II error (β error) associated with the experiment, with the aim being, the selection of sample size to reduce the β error. It is recommended to carry out the experiments with more than one replicate and then perform variance analysis to observe the change in error.

The quantitative analysis of the intermediate reaction products (monoglycerides and diglycerides) was beyond the scope of this work due to certain constraints like derivatization and the limitation of the GC column. Derivatization involves altering the compounds chemically to change their affinity towards the GC column which allows for an easier separation. But, this is a multi-step process, often introducing large error in the sample-preparation stage. Hence, an error free derivatization process needs to be developed that can easily quantify these intermediates. Further, the quantification of these intermediates can also help in improving the results of the kinetic study. Using the quantification data, it will be possible to fit kinetic models for higher order reactions.

REFERENCES

[1] (2015). Annual Energy Outlook. U.S. Energy Information Administration, Washington, DC

[2] Yuan, J. S., Tiller, K. H., Al-Ahmad, H., Stewart, N. R., & Stewart, C. N. (2008). Plants to power: bioenergy to fuel the future. Trends in Plant Science, 13(8), 421-429

[3] Demirbas, A. (2003). Biodiesel fuels from vegetable oils via catalytic and non-catalytic supercritical alcohol transesterifications and other methods: a survey. Energy conversion and Management, 44(13), 2093-2109

[4] Ma, F., Hanna, M. A. (1999). Biodiesel production: a review. Bioresource Technology, 70(1), 1-15

[5] Hanna, M. A., Isom, L., & Campbell, J. (2005). Biodiesel: current perspectives and future. Journal of Scientific and Industrial Research, 64(11), 854-857

[6] Sheehan, J., Camobreco, V., Duffield, J., Shapouri, H., Graboski, M., & Tyson, s. (2000). An overview of biodiesel and petroleum diesel life cycles (No. NREL/TP-580-24772). National Renewable Energy Lab, Golden, CO (US).

[7] Lins, C., Williamson, L. E., Leitner, S., & Teske, S. (2014). The first decade: 2004-2014, 10 years of renewable energy progress, REN21 Secretariat, Paris, France

[8] http://biodiesel.org/what-is-biodiesel/biodiesel-faq's, Biodiesel FAQ's. (2015), last accessed 8/24/2015

[9] Abbaszaadeh, A., Ghobadian, B., Omidkhah, M. R., & Najafi, G. (2012). Current biodiesel production technologies: a comparative review. Energy conversion and Management, 63, 138-148

[10] Demirbas, A. (2005). Biodiesel production from vegetable oils via catalytic and non-catalytic supercritical methanol transesterification methods. Progress in Energy and Combustion Science, 31(5-6), 466-487

[11] Bartholomew, D. (1981). Vegetable oil fuel. J. Am. Oil. Chem. Soc., 58 (4)

[12] Ramadhas, A. S., Jayaraj, S., & Muraleedharan, C. (2004). Use of vegetable oils as I.C. engine fuels – A review. Renewable Energy, 29(5), 727-742

[13] Jahirul, M. I., Rasul, M. G., Chowdhury, A. A., & Ashwath, N. (2012). Biofuels production through biomass pyrolysis – a technological review. Energies, 5(12), 4952-5001

[14] Chang, C., & Wan, S. W. (1947). China's motor fuels from tung oil. Industrial and Engineering Chemistry, 39(12), 1543-1548

[15] Aguado, R., Gaisan, B., Prieto, R., & Bilbao, J. (2003). Kinetics of polystyrene pyrolysis in a conical spouted bed reactor. Chemical Engineering Journal, 92(1), 91-99

[16] Cornelissen T., Yperman, J., Reggers, G., Schreurs, S., & Carleer, R. (2008). Flash co-pyrolysis of biomass with polylactic acid. Part 1: Influence on bio-oil yield and heating value. Fuel, 87(7), 1031-1041

[17] Sharma, M. K., & Shah D. O. (1983). Introduction to macro- and microemulsions. In ACS symposium series (No. 272, pp. 1-18). Oxford University Press

[18] Yusuf, N. N. A. N., Kamarudin, S. K., & Yaakub, Z. (2011). Overview on the current trends in biodiesel production. Energy conversion and Management, 52(7), 2741-2751

[19] Ziejewski, M., Kaufman, K. R., Schwab, A. W., & Pryde, E. H. (1984). Diesel engine evaluation of a nonionic sunflower oil-aqueous ethanol microemulsion. Journal of the American Oil Chemists' Society, 61(10), 1620-1626

[20] Ali, Y., & Hanna, M. A. (1994). Alternative diesel fuels from vegetable oils. Bioresource Technology, 50(2), 153-163

[21] Otera, J. (1993). Transesterification. Chemical Reviews, 93(4), 1449-1470

[22] Srivastava, A., & Prasad, R. (2000). Triglyceride-based diesel fuels. Renewable and Sustainable Energy Reviews, 4(2), 111-133

[23] Meher, L. C., Sagar, D. V., & Naik, S. N. (2006). Technical aspects of biodiesel production by transesterification – a review. Renewable and Sustainable Energy Reviews, 10(3), 248-268

[24] Gryglewicz, S. (1999). Rapeseed oil methyl ester preparation using heterogeneous catalysts. Bioresource Technology, 70(3), 249-253

[25] Canacki, M., & Van Gerpen, J. (1999). Biodiesel production via acid catalysts. Transactions of the ASAE – American Society of Agricultural Engineers, 42(5), 1203-1210

[26] Briand, D., Dubreucq, E., & Galzy, P. (1994). Enzymatic fatty ester synthesis in aqueous medium with lipase from Candida parapsilosis (Ashford) Langeron and Talice. Biotechnolgy Letters, 16(8), 813-818

[27] Freedman, B., Butterfield, R. O., & Pryde, E. H. (1986). Transesterifcation kinetics of soybean oil. Journal of American Oil Chemists' Society, 63(10), 1375-1380

[28] Lotero, E., Lui, Y., Lopez, D. E., Suwannakam, K., Bruce, D. A., & Goodwin, J. G. (2005). Synthesis of biodiesel via acid catalysts. Industrial and Engineering Chemistry Research, 44(14), 5353-5363

[29] Lam, M. K., Lee, K. T., & Mohamed, A. R. (2010). Homogeneous, heterogeneous and enzymatic catalysis for transesterification of high free fatty acid oil (waste cooking oil) to biodiesel: a review. Biotechnology Advances, 28(4), 500-518

[30] Wang, Y., Ou, S., Liu, P., Xue, F., & Tang, S. (2006). Comparison of two different processes to synthesize biodiesel by waste cooking oil. Journal of Molecular Catalysis A: Chemical, 252(1-2), 107-112

[31] Felizardo, P., Correia, M. J. N., Raposo, I., Mendes, J. F., Berkemeier, R., & Bordado, J. M. (2006). Production of biodiesel from waste frying oils. Waste Management, 26(5), 487-494

[32] Zabeti, M., Daud, W. M. A. W., & Aroua, M. K. (2009). Activity of solid catalysts for biodiesel production: a review. Fuel Processing Technology, 90(6), 770-777

[33] Kouzu, M., Kasuno, T., Tajika, M., Sugimoto, Y., Yamanaka, S., & Hidaka, J. (2008). Calcium oxide as a solid base catalyst for transesterification of soybean oil and its application to biodiesel production. Fuel, 87(12). 2798-2806

[34] Di Serio, M., Ledda, M., Cozzolino, M., Minutillo, G., Tesser, R., & Santacesaria, E. (2006). Transesterification of soybean oil to biodiesel by using heterogeneous basic catalyst. Industrial & Engineering Chemistry Research, 45(9), 3009-3014

[35] Liu, X., He, H., Wang, Y., & Zhu, S. (2007). Transesterification of soybean oil to biodiesel using SrO as a solid base catalyst. Catalysis Communications, 8(7), 1107-1111.

[36] Kulkarni, M. G., & Dalai, A. K., (2006). Waste cooking oil an economic source for biodiesel: a review. Industrial and & Engineering Chemistry Research, 45(9), 2901-2913.

[37] Jitputti, J., Kitiyanan, B., Rangsunvigit, P., Bunyakiat. K., Attanatho, L., & Jenvanitpankajul, P. (2006). Tranesterification of crude palm kernel oil and coconut oil by different solid catalysts. Chemical Engineering Journal, 116(1), 61-66.

[38] Ranganathan, S. V. Narasimhan, S. L., & Muthukumar, K. (2008). An overview of enzymatic production of biodiesel. Bioresource Technology, 99(10), 3975-3981.

[39] Mittelbach, M. (1990). Lipase catalyzed alcoholysis of sunflower oil. Journal of the American Oil Chemists' Society, 67(3), 168-170.

[40] Bajaj, A., Lohan, P., Jha, P. N., Mehrotra, R. (2010). Biodiesel production through lipase catalyzed transesterification: An overview. Journal of Molecular Catalysis B: Enzymatic, 62(1), 9-14.

[41] Cagniard De La Tour, C. (1822). Presentation of some results obtained by the combined action of heat and compression on certain liquids, such as water, alcohol, ether [i.e., diethyl ether], and distilled petroleum spirit. Annales de Chimie et de Physique, 21(2), 127-132.

[42] Darr. J. A., & Poliakoff. M. (1999). New directions in inorganic and metal-organic coordination chemistry in supercritical fluids. Chemical Reviews, 99(2), 495-542.

[43] Ngamprasertsith, S., & Sawangkeaw, R. (2011). Transesterification in supercritical conditions. Biodiesel Feedstocks and Processing Technologies, Rejika: InTech, 247-268.

[44] Kemmere, M. F., & Meyer, T. (Eds.). (2006). Supercritical carbon dioxide in polymer reaction engineering,, John Wiley & Sons, Weinheim, Germany.

[45] Clifford, A., & Clifford, T. (1999). Fundamentals of Supercritical Fluids, Oxford University Press.

[46] Arai, Y., Sako, Y., & Takebayashi, Y. (Eds). (2013). Supercritical fluids molecular interactions, physical properties and new applications. Springer Science & Business Media.

[47] Daisakou, M., Louloudi, A; & Papayannakos, N. (1998). Kinetics of the non-catalytic transesterification of soybean oil. Fuel, 77(12), 1297-1302

[48] Saka, S., & Kusdiana, D. (2001). Biodiesel fuel from rapeseed oil as prepared in supercritical methanol. Fuel, 80(2), 225-231

[49] Kusdiana, D., & Saka, S. (2001). Kinetics of transesterification in rapeseed oil to biodiesel fuel as treated in supercritical methanol. Fuel, 80(5), 693-698

[50] Song, E., Lim, J., Le, H., & Lee, Y. (2008). Transesterification of RBD palm oil using supercritical methanol. The Journal of Supercritical Fluids, 44(3), 356-363

[51] He, H., Sun, S., Wang, T., & Zhu, S. (2007). Transesterification kinetics of soybean oil for production of biodiesel in supercritical methanol. Journal of the American Oil Chemists' Society, 84(4), 399-404

[52] Bernal, J. M., Lozano, P., Garcia-Verdugo, E., Burguet, M. I., Sanchez-Gomez, G., Lopez-Lopez, G., Pucheault, M., Vaultier, M., & Luis, S. V. (2012). Supercritical synthesis of biodiesel. Molecules, 17(7), 8696-8719

[53] Bunyakiat, K., Makmee, S., Sawangkeaw, R., & Ngamprasertsith, S. (2006). Continuous production of biodiesel via transesterification from vegetable oils in supercritical methanol. Energy & Fuels, 20(2). 812-817.

[54] Demirbas, A. (2002). Biodiesel from vegetable oils via transesterification in supercritical methanol. Energy Conversion & Management, 43(17), 2349-2356

[55] Kusdiana, D., & Saka, S. (2004). Effects of water on biodiesel fuel production by supercritical methanol treatment. Bioresource Technology, 91(3), 289-295

[56] Vietez, I., Pardo, M. J., Da Silva, C., Bertoli, C., De Castilhos, F., Oliveira, J. V., Grompone, M. A., & Jachmanian, I. (2011). Continuous synthesis of castor oil ethyl esters under supercritical ethanol. The Journal of Supercritical Fluids, 56(3), 271-276

[57] Diaz, M. S., Espinosa, S., & Brignole, E. A. (2009). Model-based cost minimization in non-catalytic biodiesel production plants. Energy & Fuels, 23(11), 5587-5595

[58] Marchetti, J. M., & Errazu, A. F. (2008). Technoeconomic study of supercritical biodiesel production plant. Energy Conversion and Management, 49(8), 2160-2164.

[59] Haas, M. J., McAloon, A. J., Yee, W. C., & Foglia, T. A. (2006). A process model to estimate biodiesel production costs. Bioresource Technology, 97(4), 671-678

[60] Ahmad, A., Yasin, N. M., Derek, C., & Lim, J. (2011). Microalgae as a sustainable energy source for biodiesel production: a review. Renewable and Sustainable Energy Reviews, 15(1), 584-593

[61] Canakci, M. (2007). The potential of restaurant waste lipids as biodiesel feedstocks. Bioresource Technology, 98(1), 183-190

[62] Barnwal, B. K., & Sharma, M. P. (2005). Prospects of biodiesel production from vegetable oils in India. Renewable and Sustainable Energy Reviews, 9(4), 363-378

[63] Issariyakul, T., & Dalai, A. K. (2014). Biodiesel from vegetable oils. Renewable and Sustainable Energy Reviews, 31, 446-471

[64] Chhetri, A. B., Watts, K. C., & Islam, M. R. (2008). Waste cooking oil as an alternate feedstock for biodiesel production. Energies, 1(1), 3-18

[65] Nawar, W. W. (1984). Chemical changes in lipids produced by thermal processing. Journal of Chemical Education, 61(4), 299

[66] Mittelbach, M., & Enzelsberger, H. (1999). Transesterification of heated rapeseed oil for extending diesel fuel. Journal of the American Oil Chemists' Society, 76(5), 545-550

[67] Zheng, D., & Hanna, M. (1996). Preparation and properties of methyl esters of beef tallow. Bioresource Technology, 57(2), 137-142

[68] Karmarkar, A., Karmarkar, S., & Mukherjee, S. (2010). Properties of various plants and animals feedstocks for biodiesel production. Bioresource Technology, 101(19), 7201-7210

[69] Marulanda, V. E., Anitescu, G., & Tavlarides, L. L. (2009). Biodiesel fuels through a continuous flow process of chicken fat supercritical transesterification. Energy & Fuels, 24(1), 253-260

[70] Lebedevas, S., Vaicekauskas, A., Lebedeva, G., Makareviciene, V., Janulis, P., & Kazancev, K. (2006). Use of waste fats of animal and vegetable origin for the production of biodiesel fuel: quality, motor properties, and emissions of harmful components. Energy & fuels, 20(5), 2274-2280.

[71] Öner, C., & Altun, Ş. (2009). Biodiesel production from inedible animal tallow and an experimental investigation of its use as alternative fuel in a direct injection diesel engine. Applied Energy, 86(10), 2114-2120.

[72] Mata, T. M., Martins, A. A., & Caetano, N. S. (2010). Microalgae for biodiesel production and other applications: a review. Renewable and Sustainable Energy Reviews, 14(1), 217-232

[73] Suen, Y., Hubbard, J. S., Holzer, G., & Tornabene, T. G. (1987). Total lipid production of the green alga Nannochloropsis Sp. QII under different nitrogen regimes. Journal of Phycology, 23(s2), 289-296.

[74] Grima, E. M., Belarbi, E. H., Fernández, F. A., Medina, A. R., & Chisti, Y. (2003). Recovery of microalgal biomass and metabolites: process options and economics. Biotechnology advances, 20(7), 491-515.

[75] Halim, R., Danquah, M. K., & Webley, P. A. (2012). Extraction of oil from microalgae for biodiesel production: a review. Biotechnology advances, 30(3), 709-732.

[76] Uduman, N., Qi, Y., Danquah, M. K., Forde, G. M., & Hoadley, A. (2010). Dewatering of microalgal cultures: a major bottleneck to algae-based fuels.Journal of renewable and sustainable energy, 2(1), 012701.

[77] Yanfen, L., Zehao, H., & Xiaoqian, M. (2012). Energy analysis and environmental impacts of microalgal biodiesel in China. Energy Policy, 45, 142-151.

[78] Lardon, L., Helias, A., Sialve, B., Steyer, J. P., & Bernard, O. (2009). Life-cycle assessment of biodiesel production from microalgae. Environmental science & technology, 43(17), 6475-6481.

[79] Montgomery, D. C., & Montgomery, D. C. (1984). Design and analysis of experiments (Vol. 7). New York: Wiley.

[80] Pietrzyk, D. J., & Frank, C. W. (1979). Development of an analytical method (Edition 2). New York: Academic Press.

[81] Barwick, V. (2003). Preparation of calibration curves – A guide to best practices. LGC Limited.

[82] Foggler Scott, H. (2010). Elements of Chemical Reaction Engineering (Edition 4). Prentice Hall International Series in the Physical and Chemical Engineering Sciences. Boston, MA.

[83] Sunol, A. K., & Sunol, S. G. (2001). Safer solvents and processes, Handbook of Solvents (Edition 2, 2014), Ed. Wypych, G., Chem Tech Publishing.

[84] Sunol, A. K., Sunol, S. G., & Aslam, N. (2005). Supercritical fluid technology – reactions, Ed. Sunggyu Lee, C. W., Encyclopedia of Chemical Processing (ECHP), Marcel Dekker, Inc.

APPENDIX A: LIST OF NOMENCLATURE

df: Degrees of freedom

FAME: Fatty Acid Methyl Ester

FFA's: Free Fatty Acids

GC-MS: Gas Chromatography-Mass Spectrometry

HPLC: High Performance Liquid Chromatography

MTOF: Mass Time of Flight

MS-QTOF: Mass Spectrometry-Qualitative Time of Flight

OECD: Organization for Economic Co-operation and Development

PID: Proportional-Integral-Derivative

SCF: Supercritical Fluid

APPENDIX B: ELECTRON IONISATION SPECTRA FOR METHYL ESTERS

B.1 Relative Size of Biodiesel Peaks

As seen in the figure below, some peaks are significantly larger. The peaks of palmitic acid methyl ester, stearic acid methyl ester, oleic acid methyl ester and linoleic acid methyl ester are tall, sharp and large in area, reflecting their substantial presence in the biodiesel sample. On the other hand the smaller peaks of linolenic acid methyl ester, eicosanoic acid methyl ester and 9-cis-11-trans-octadecadanoic acid methyl ester indicate the presence of these methyl esters in trace amounts.

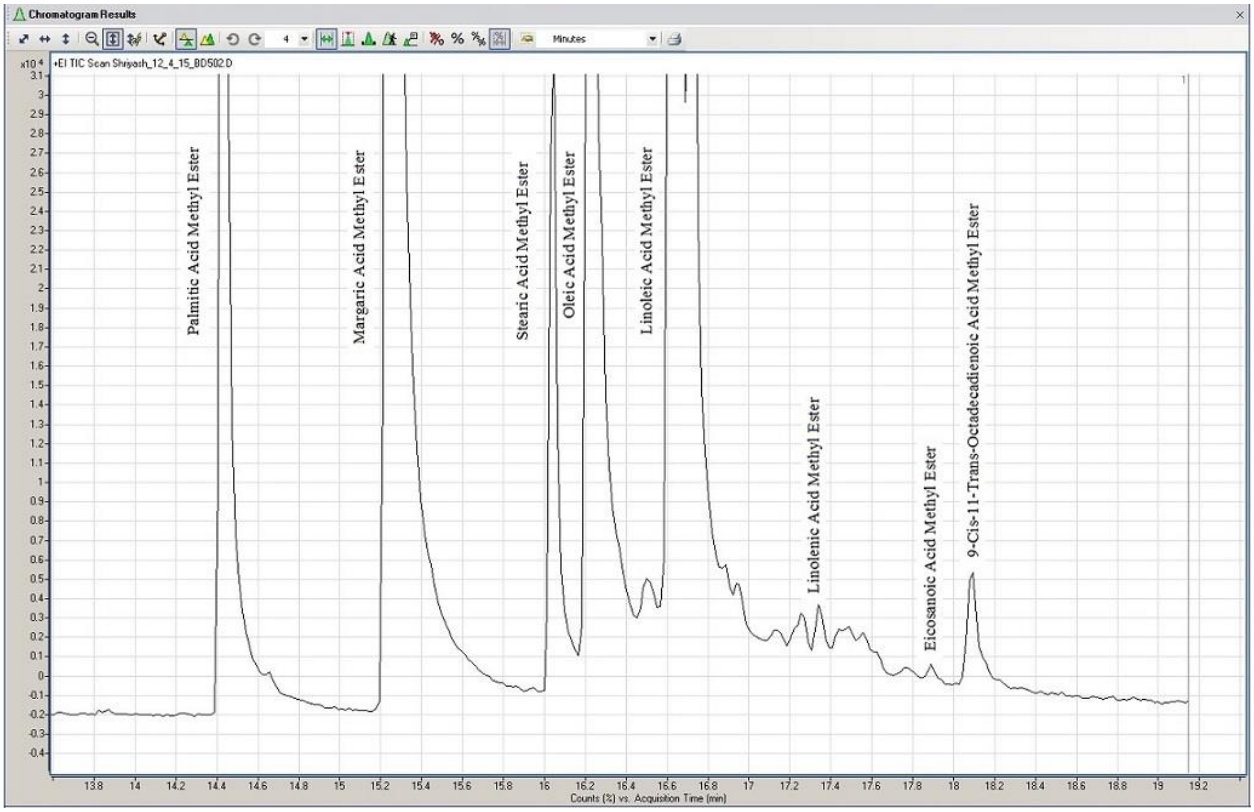

Figure B-1 Relative size of peaks

B.2 Electron Ionization (EI) Spectra for Methyl Esters

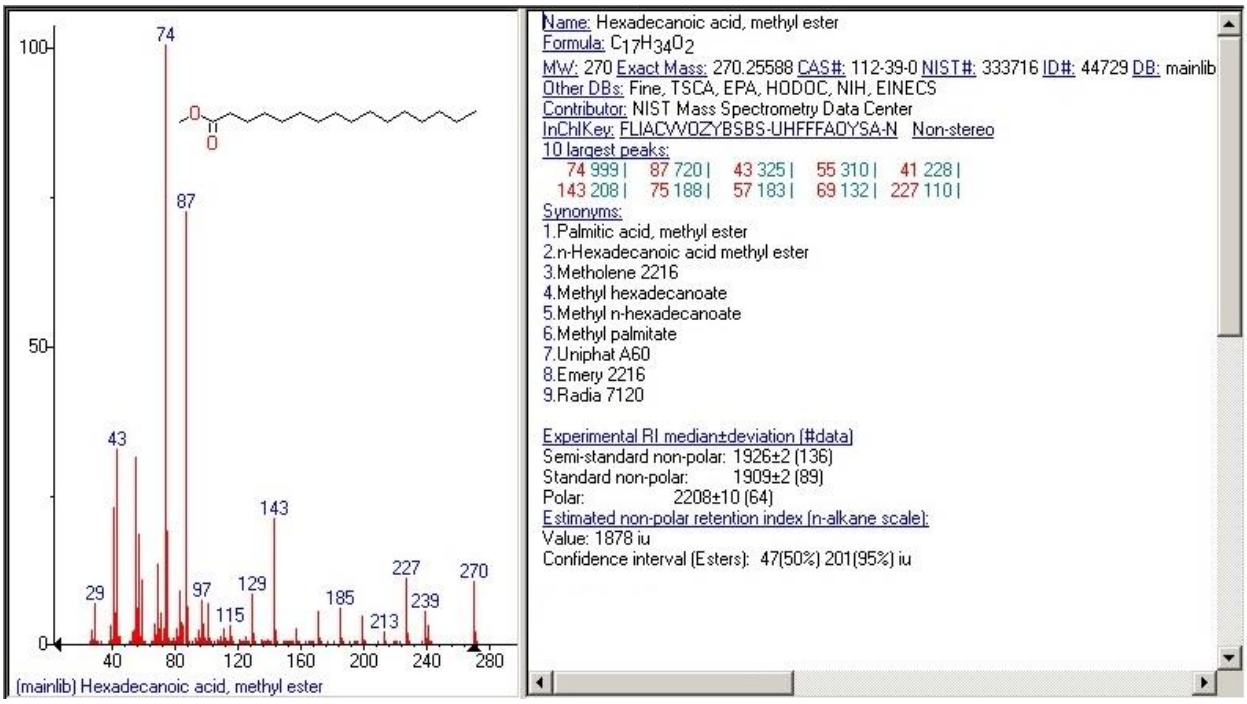

Figure B-2 EI Spectra for Palmitic acid methyl ester

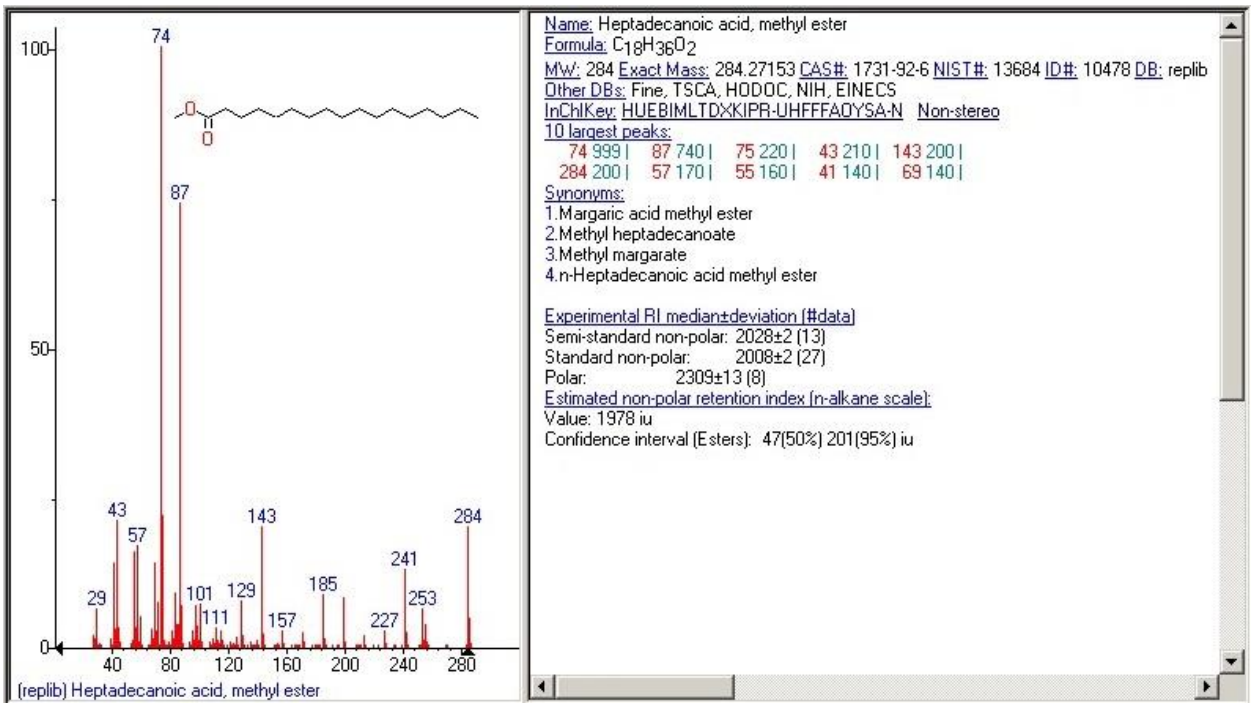

Figure B-3 EI Spectra for Margaric acid methyl ester (internal standard)

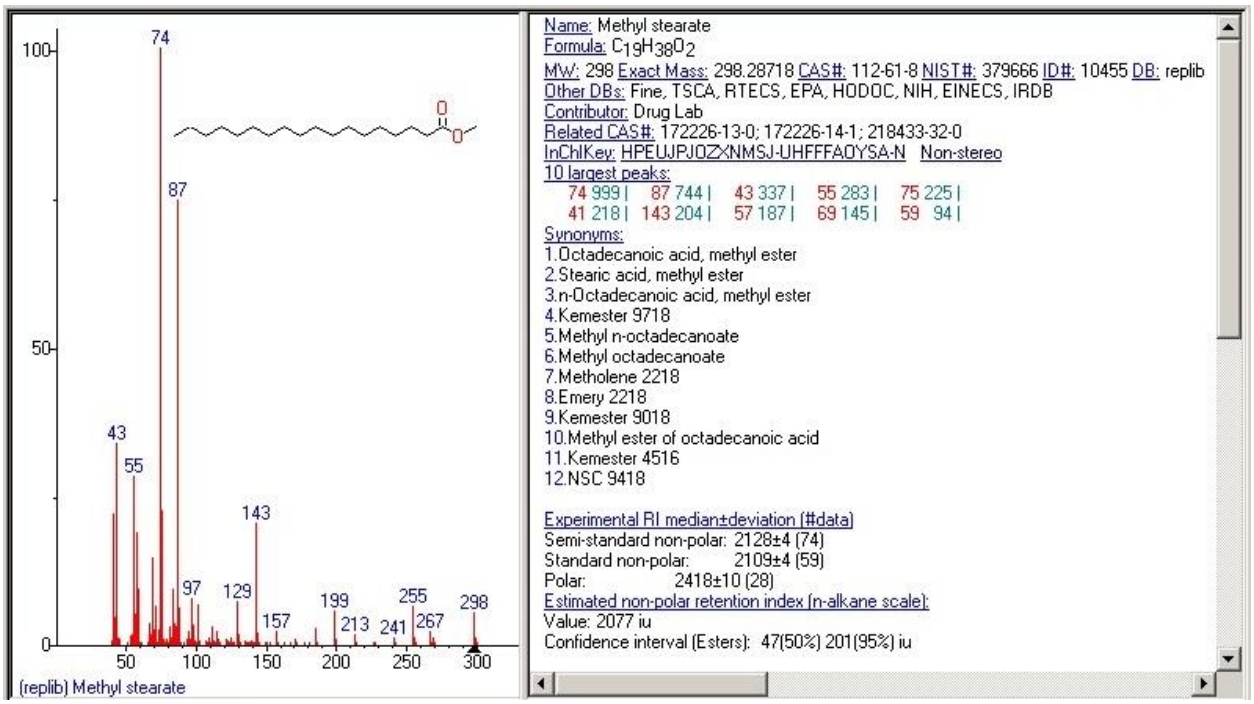

Figure B-4 EI Spectra for Stearic acid methyl ester

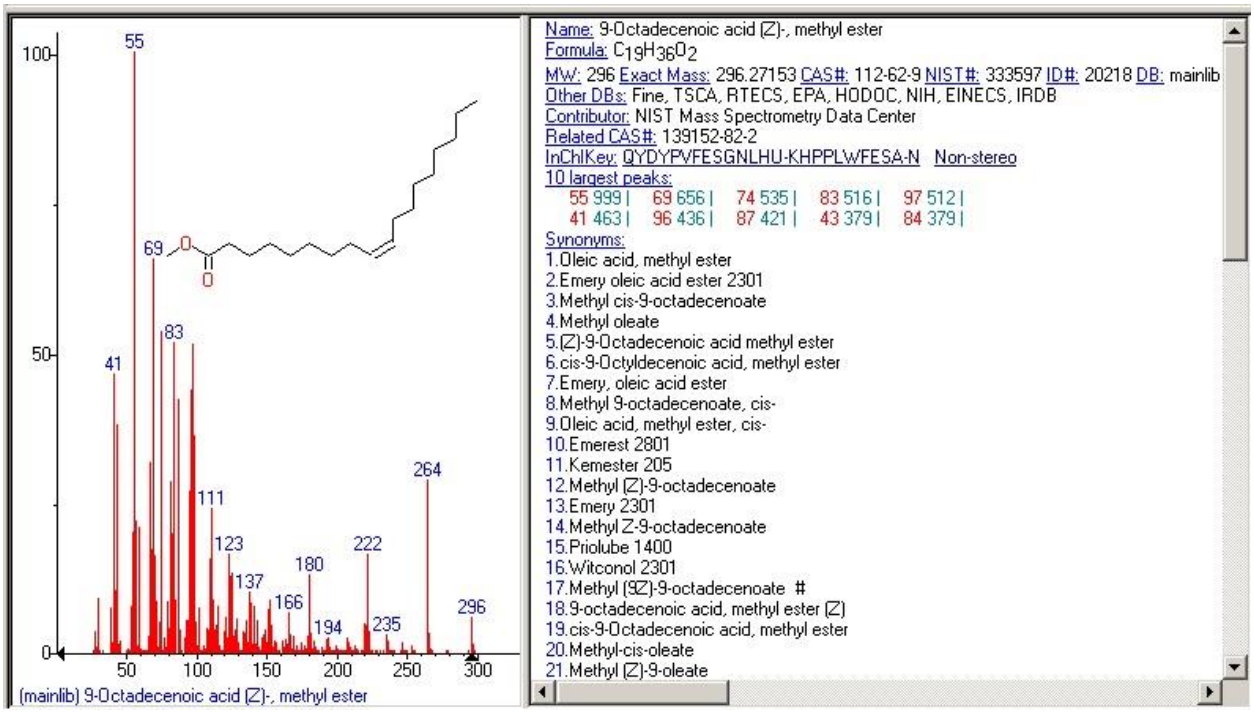

Figure B-5 EI Spectra for Oleic acid methyl ester

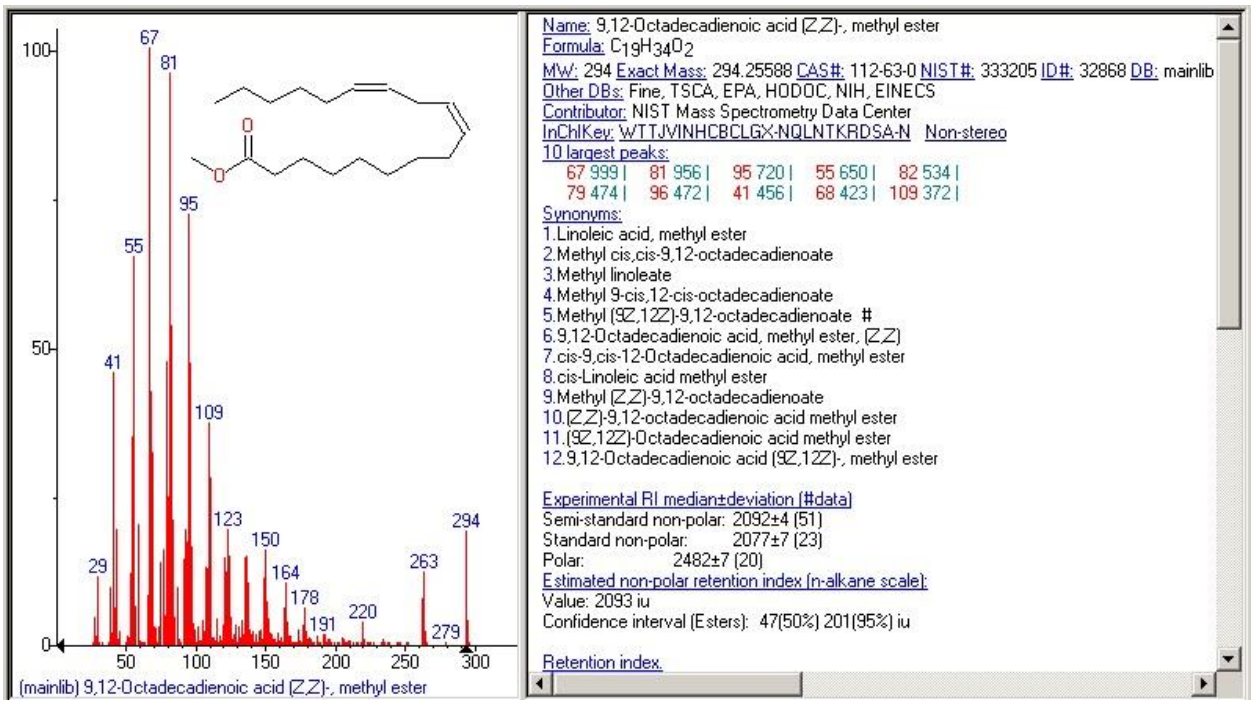

Figure B-6 EI Spectra for Linoleic acid methyl ester

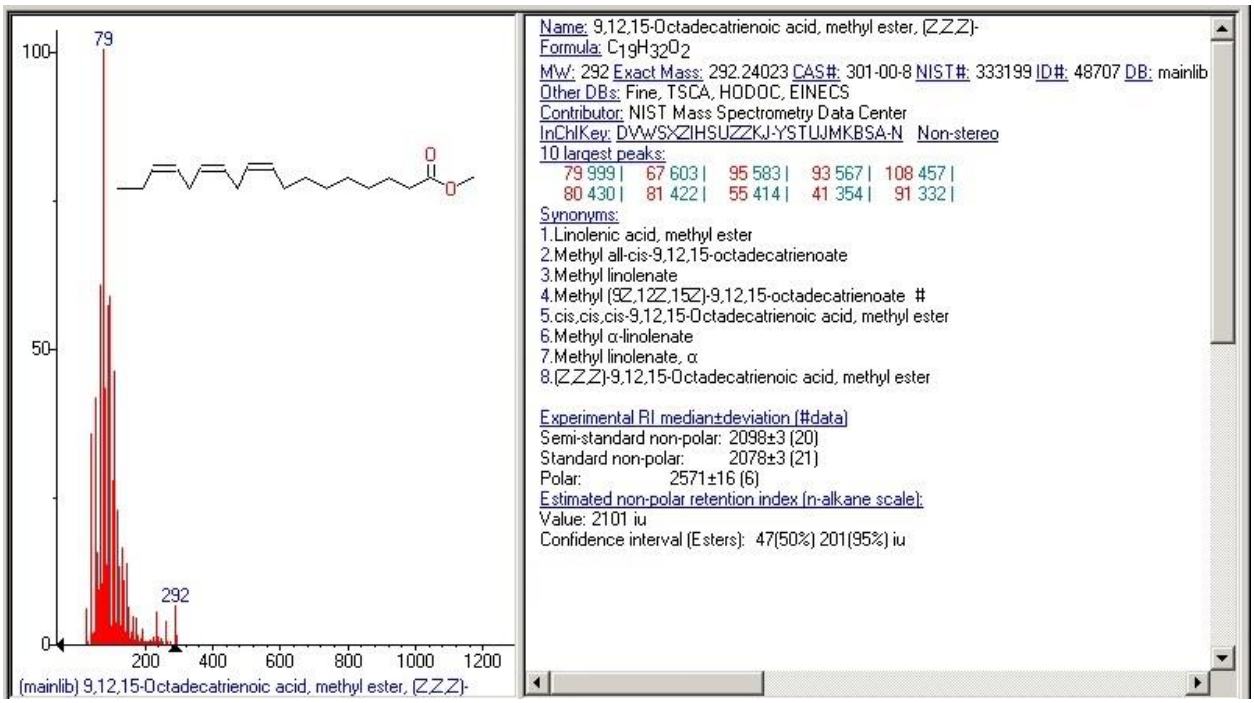

Figure B-7 EI Spectra for Linolenic acid methyl ester

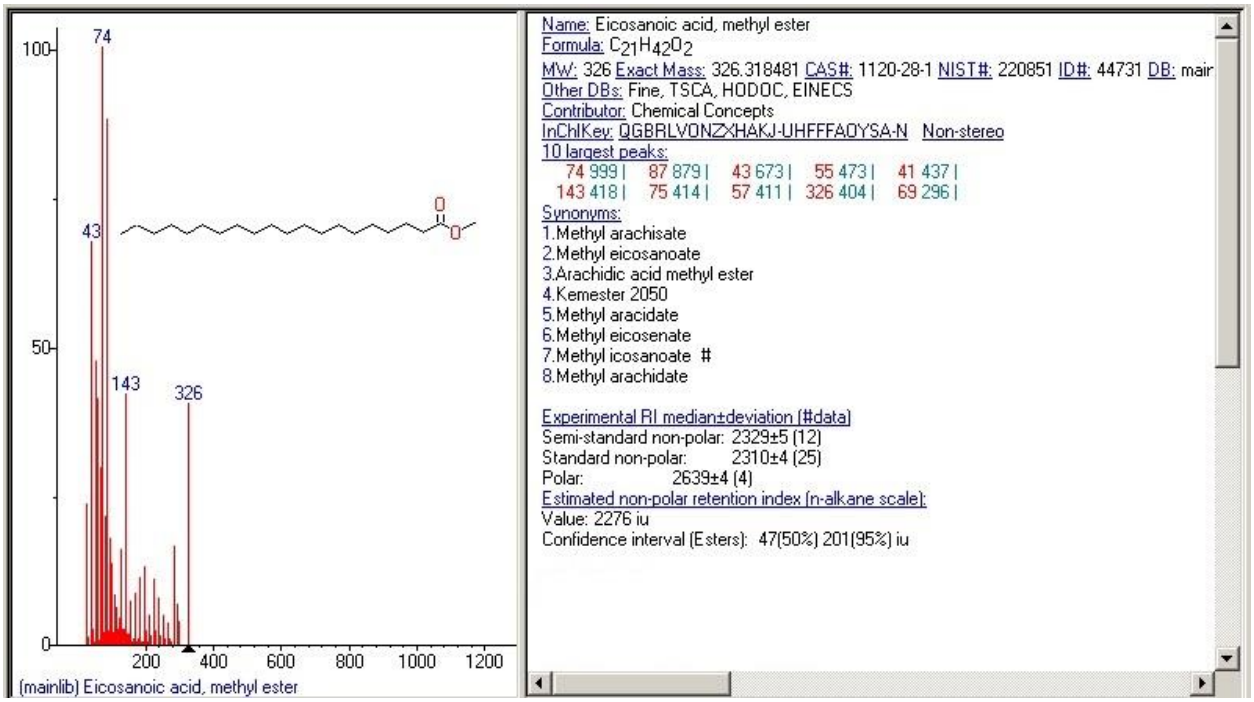

Figure B-8 EI Spectra for Eicosanoic acid methyl ester

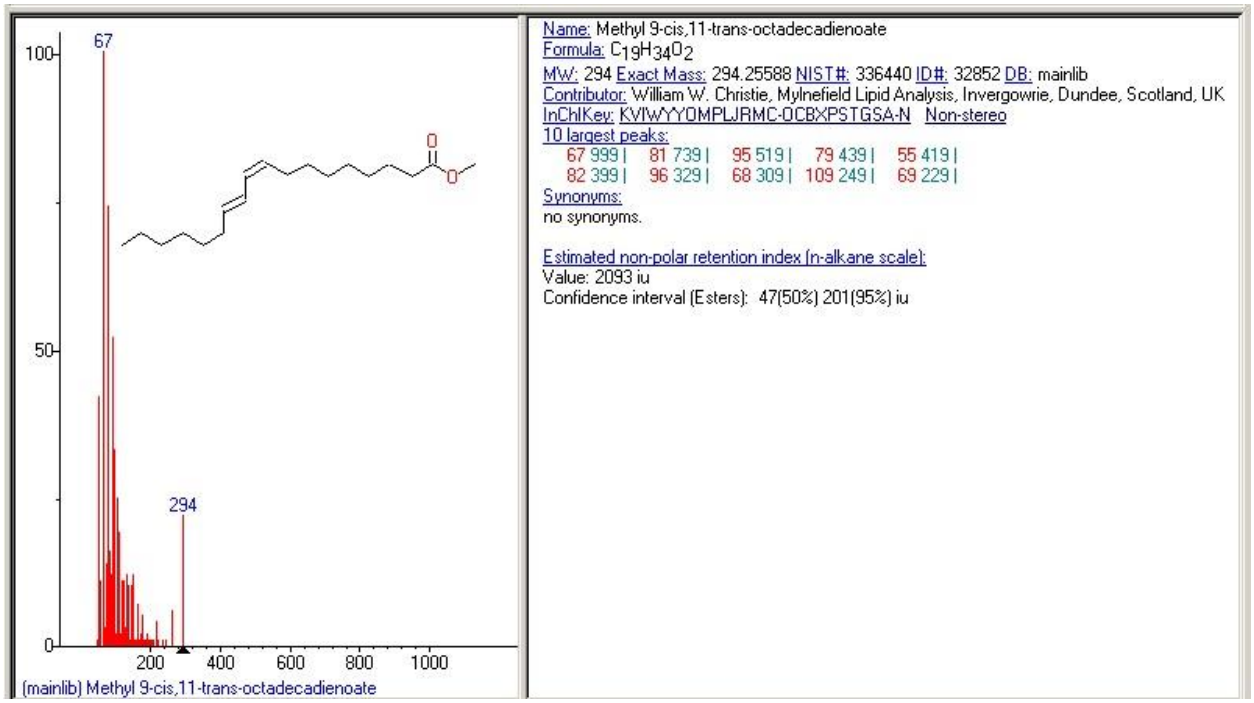

Figure B-9 EI Spectra for 9-Cis-11-Trans-Octadecadenoic acid methyl ester

APPENDIX C: CALCULATIONS

C.1 Biodiesel Yield Calculation Methodology

The yield calculations for the 50 minute sample collected from the experiment at 325 °C and 43:1 molar ratio are shown below. First, the peak areas were obtained by integrating the chromatogram.

Table C-1 Peak areas for methyl esters

325 °C, 43:1 molar ratio, 50 minute sample, replicate 1					
Peak	Palmitic Acid Methyl Ester	Margaric Acid Methyl Ester	Stearic Acid Methyl Ester	Oleic Acid Methyl Ester	Linoleic Acid Methyl Ester (and other minor ester peaks)
Retention Time	14.446	15.267	16.054	16.239	16.641
Peak Area	99201506	555735630	44721954	279648553	378097506
325 °C, 43:1 molar ratio, 50 minute sample, replicate 2					
Peak	Palmitic Acid Methyl Ester	Margaric Acid Methyl Ester	Stearic Acid Methyl Ester	Oleic Acid Methyl Ester	Linoleic Acid Methyl Ester (and other minor ester peaks)
Retention Time	14.477	15.268	16.055	16.24	16.642
Peak Area	95135277	535508636	50390037	298992220	393752939

The peak areas were added together, except for the area of the internal standard. The concentration was then calculated by using the area and the equation of the calibration plot, which is:

$$Area = (4 * 10^{6}) * Concentration - (1 * 10^{-8}) \quad \text{(C.1.1)}$$

This concentration was then divided by the known concentration of the samples noted during sample preparation. The resulting value when multiplied by 100, gave the methyl ester yield. The table below gives the total peak areas, their corresponding concentrations from the calibration plot equation and the final yield of biodiesel.

Table C-2 Yield of biodiesel

Replicate	***Total Area***	***Concentration Calculated***	***Concentration Prepared***	***Yield***	***Average Yield***
1	801669519	200.41738	205.70062	97.431587	97.26406
2	838270473	209.56762	215.83431	97.096527	

C.2 Coded Variables

$$Coded\ Value = \frac{Actual\ value - (mean\ of\ the\ range)}{\left({Difference\ in\ range}/{2}\right)} \qquad \text{(C.2.1)}$$

For the range 310 °C ≤ T ≤ 325 °C and 43:1 ≤ Molar Ratio ≤ 30:1 the coded values can be calculated using the above formula as,

$$Coded\ value\ for\ 325\ °C\ = \frac{325 - ((325 + 310)/2)}{(325 - 310)/2} = +1$$

$$Coded\ value\ for\ 310\ °C\ = \frac{310 - ((325 + 310)/2)}{(325 - 310)/2} = -1$$

$$Coded\ value\ for\ molar\ ratio\ 43\ = \frac{43 - ((43 + 30)/2)}{(43 - 30)/2} = +1$$

$$Coded\ value\ for\ molar\ ratio\ 30\ = \frac{30 - ((43 + 30)/2)}{(43 - 30)/2} = -1$$

C.3 Analysis of Variance (ANOVA) Calculations

From the ANOVA table the yield was summed together. In this case we have 4 main experiments, implies N = 4, and one replicate each, implies n = 1.

Table C-3 ANOVA table with sum of output

Treatment	Main Factors		Interaction	Output
	T	***MR***	***T*MR***	***Yield (50 min)***
Both Low	-1	-1	1	83.47098
Molar Ratio (MR) high	-1	1	-1	94.95858
Temperature (T) high	1	-1	-1	87.44034
Both high	1	1	1	97.26406
Total				**363.134**

Predefined functions in Microsoft Excel were used for calculating the contrast, effect and sum of squares for temperature:

$$Contrast = SUMPRODUCT(Array\ T, Array\ Yield) \tag{C.3.1}$$

$$Effect = \frac{1}{\frac{Total\ experiments}{2} * n} * (contrast) \tag{C.3.2}$$

$$Sum\ of\ Squares = \frac{1}{Total\ experiments * n} * (contrast^2) \tag{C.3.3}$$

$$Mean\ Square\ (MS) = \frac{Sum\ of\ Squares}{d.f.} \tag{C.3.4}$$

Similar calculations follow for molar ratio and the interaction.

The total sum of squares can be calculated as:

$$Total\ Sum\ of\ Squares = SUMSQ(Array\ Yield) - (Total^2/N) \tag{C.3.5}$$

There are three degrees of freedom associated with the 2^2 design, one each with the main effects, and one with the interaction. Using these, the mean squares can be calculated as shown below.

Table C-4 Contrasts, effects, sum of squares and mean squares for the factors and interactions

Parameter	***T***	***MR***	***T*MR***	***Total***
Contrasts	6.274837	21.31131	-1.66388	-
Effects	3.137419	10.65566	-0.83194	-
Sum of Squares	9.843395	113.543	0.692127	124.0785
df	1	1	1	-
Mean Squares	9.843395	113.543	0.692127	-

The next step was to find the mean square of error. Since n = 1, the degrees of freedom would be zero and the above equation becomes invalid to determine the mean square of error. With one replicate there is no internal estimate of error. In order to estimate the error, we can plot the effects ordered from low to high versus their corresponding z-values, where,

$$Z\ value = NORMSINV((j - 0.5)/N) \quad \text{(C.3.6)}$$

This is known as a normal probability plot. The small effects will have a mean of zero and tend to lie on a straight line. These effects can be clubbed together as an error estimate. The significant effects will have non-zero means and will not lie on the straight line. In mathematical representation, a line is plotted incorporating points that lie as close to each other as possible (ideally joining the 25^{th} and 75^{th} percentile, but in this case the closest points are clubbed together). The sum of squares corresponding to these points can be combined together to represent the sum of squares of the error. The calculations are shown in the table below:

Table C-5 Calculations for z-value

Effects	***Ordered Effects***	***j***	***(j-0.5)/3***	***Z***
3.137419	-0.83194	1	0.166667	-0.96742
10.65566	3.137419	2	0.5	0
-0.83194	10.65566	3	0.833333	0.967422

The normal probability plot is as shown in figure C-1.

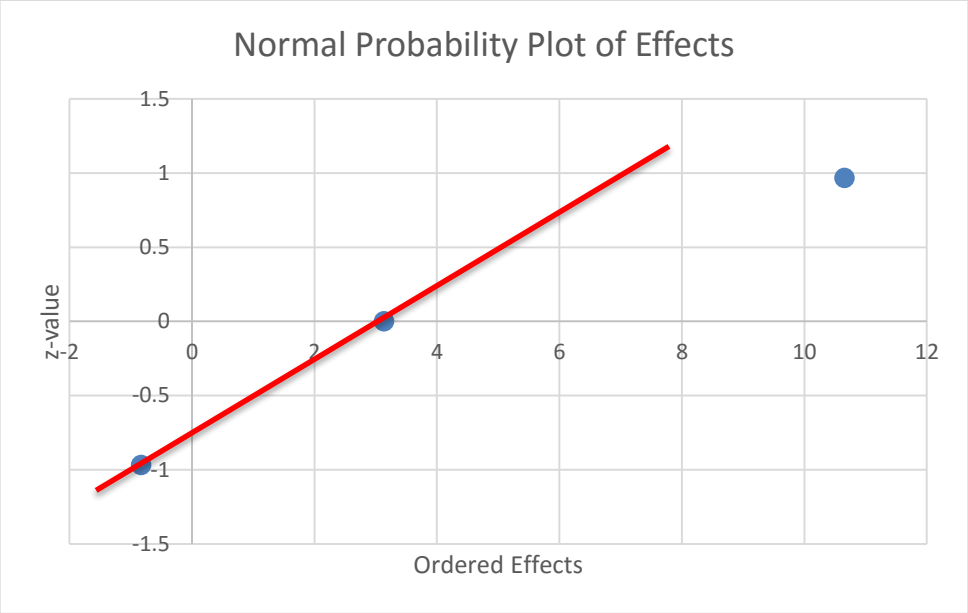

Figure C-1 Normal probability plot of effects

It is clear from the plot that the sum of squares for the temperature and the interaction can be combined together as the sum of squares of error. Thus, mean square error is 5.2373. The mean square values for the treatment and the error can then be used to calculate F_0

$$F_0 = \frac{Mean\ Square_{treatment}}{Mean\ Square_{error}} \tag{C.3.7}$$

The significance of the factor or interaction can be then validated if the F_0 value is greater than the $F_{critical}$ value, where the $F_{critical}$ value can be calculated from the FINV function in Excel.

$$F_{critical} = FINV(\alpha, d.f.1, d.f.2) \tag{C.3.8}$$

Here α represents the type 1 error (alpha error) which is fixed before starting the calculations. The alpha error can be related to the confidence level. In other words, α = 0.05 represents a 95% confidence level. All the calculations in this work are made with α = 0.05. The d.f. 1 equals 1 (for the treatment) while the d.f. 2 equals 2 (for the error). The table below gives the values for F_0 and $F_{critical}$, and the significant factor is shown in bold.

Table C-6 F-test to determine significance

F-Test	Temperature	Molar Ratio	Interaction
F_0	1.868611	**21.55432**	0.131389
$F_{critical}$	18.51282	18.51282	18.51282

Once the significant factors have been identified, the regression equation can be built with the regression coefficients (Betas). The regression model for a 2^2 experiment is,

$$y = \beta_0 + \beta_1 x_1 + \beta_2 x_2 + \beta_3 x_1 x_2 \quad \text{(C.3.9)}$$

where,

$$\beta_0 = AVERAGE(Yield)$$

$$\beta_1 = \beta_2 = (Factor\ Effect)/2$$

$$\beta_3 = (Interaction\ Effect)/2$$

Since only the molar ratio (β_2 term) is statistically significant, the other terms can be dropped from the equation.

Thus, the regression equation is,

$$Yield = 90.78 + 5.32 * (Molar\ Ratio)$$

It is important to note that the molar ratio value in the above equation is in terms of its coded variables.

C.4 Test for Non-Linearity of the Model

The regression model is built under the assumption that the output linearly changes with the change in molar ratio. We need to confirm the linearity of the model. We can do so by using the center point approach. Let n_c be the center point observations, n_f be the factorial design observations, y_i be the center point data, y_F be the average of four runs at the factorial points, y_c average of the data collected at center points. These terms being defined, the quadratic curvature of the model can be confirmed is the difference $y_F - y_c$ is large. The sum of squares for pure quadratic effect is given by,

$$SS_{Pure\ quadratic} = \frac{n_f n_c (y_F - y_c)^2}{n_F + n_C} \quad \text{(C.4.1)}$$

Mean squares for pure quadratic effect and error are:

$$MS_{Pure\ quadratic} = \frac{SS_{Pure\ quadratic}}{d.f.} \quad \text{(C.4.2)}$$

$$MS_E = \frac{SS_E}{n_C - 1} = \frac{\sum (y_i - y_c)^2}{n_C - 1} \quad \text{(C.4.3)}$$

The F_0 can be calculated using these values, and compared with $F_{critical}$ to determine the significance of the quadratic effect. The results are shown in table 6-4.

C.5 Calculations for Arrhenius Plot

The Arrhenius plot can be generated using the values of rate constants for the forward reaction obtained from the non-linear regression, and the corresponding temperatures. As shown in the table below, (1/T) is calculated for each of the reaction conditions. These are then plotted against the natural log of the rate constant values to generate the Arrhenius plot. The values of the activation energy and the pre-exponential factors can be calculated from the equation of the trendline of this plot.

Table C-7 Calculations for Arrhenius plot

k_f (sec^{-1})	T (K)	Molar Ratio	ln k_f	1/T (K^{-1})	1/T, ($K^{-1}*10^3$)
0.00415	598.15	43:1	-5.4839	0.00167	1.67182
0.00382	583.15	43:1	-5.5683	0.00171	1.71482
0.00350	590.65	36.5:1	-5.6546	0.00169	1.69305
0.00336	598.15	30:1	-5.6946	0.00167	1.67182
0.00333	583.15	30:1	-5.7052	0.00171	1.71482